Evaluation of the predictive ability of two elastic-viscoplastic constitutive models

Sean D. Hinchberger and R. Kerry Rowe

Abstract: Two elastic-viscoplastic constitutive formulations are evaluated using laboratory and field data from Sackville, New Brunswick and Gloucester, Ontario. Both constitutive models have been implemented in a finite element program and formulated for undrained analysis and fully coupled analysis based on Biot consolidation theory. A laboratory study of the rate-sensitive behaviour of Sackville clay is described. The response of Sackville clay during consolidated anisotropic undrained (CAU) triaxial creep, CAU triaxial compression, and incremental oedometer consolidation is compared with the calculated behaviour. The comparisons demonstrate the general ability of three-parameter elastic-viscoplastic constitutive models to satisfactorily describe the rate-dependent behaviour of Sackville clay. The measured response of Gloucester clay during long-term Rowe cell consolidation tests is compared with the calculated behaviour, and the predictive ability of both constitutive formulations is evaluated using the field performance of the Gloucester case record. In undertaking the present study, the predictive ability of two elastic-viscoplastic constitutive models is examined for two soft clays. A new method of overstress measurement is introduced for elliptical yield surfaces and the importance of adopting a scalable yield surface for the constitutive modeling of soft clay is demonstrated. A model that is suitable for the study of reinforced and unreinforced embankments on soft rate-sensitive clay foundations is identified.

Key words: elastic-viscoplastic, finite element analysis, overstress viscoplasticity, case study, rate-sensitive, coupled analysis.

Résumé : On évalue deux formulations de comportement élasto-visco-plastique au moyen de données de laboratoire et de terrain de Sackville, Nouveau-Brunswick, et de Gloucester, Ontario. Les deux modèles de comportement ont été mis en application dans un programme d'éléments finis et formulés pour une analyse non drainée et une analyse complètement couplée basée sur la théorie de consolidation de Biot. On décrit une étude en laboratoire du comportement sensible à la vitesse de déformation de l'argile de Sackville. La réaction de l'argile de Sackville durant des essais triaxiaux CAU en fluage et en compression, et des essais de consolidation oedométrique sont comparés avec le comportement calculé. Les comparaisons démontrent l'habilité générale de modèles de comportement élasto-visco-plastique à trois paramètres pour prédire de façon satisfaisante le comportement en fonction de la vitesse de déformation de l'argile de Sackville. La réaction mesurée de l'argile de Gloucester au cours d'essais de consolidation de Rowe à long terme est comparée avec le comportement calculé, et l'habilité de prédiction des deux formulations constitutives est évaluée au moyen de la performance en nature d'une histoire de cas de l'argile de Gloucester. En entreprenant la présente étude, l'habilité de prédiction de deux modèles élasto-visco-plastiques de comportement est examinée pour deux argiles molles. Une nouvelle méthode de mesure de surcontrainte est introduite pour des surfaces de limite élastique elliptiques et on démontre l'importance d'adopter une surface de limite élastique qui peut être prise à l'échelle pour la modélisation de comportement de l'argile molle. On identifie un modèle qui convient à l'étude de remblais armés ou non armés sur des fondations d'argile molle sensible à la déformation.

Mots clés : élasto-visco-plastique, analyse en éléments finis, visco-plasticité de surcontrainte, étude de cas, sensible à la déformation, analyse couplée.

[Traduit par la Rédaction]

Introduction

Predicting the engineering response of soft rate-sensitive clay can be difficult (e.g., Folkes and Crooks 1985; Rowe and Hinchberger 1998; Zhu et al. 2001). In many countries, infrastructure development depends on the successful design and construct of embankments on these difficult soils. Typically, the rate-sensitive characteristics of cohesive soils are neglected, and the performance of embankments constructed on these deposits is assessed using the theories of

Received 15 September 2004. Accepted 20 September 2005. Published on the NRC Research Press Web site at http://cgj.nrc.ca on 6 December 2005.

S.D. Hinchberger.[1] Department of Civil and Environmental Engineering, The University of Western Ontario, London, ON N6A 5B9, Canada.
R.K. Rowe. Queen's University, Kingston, ON K7L 3N6, Canada.

[1]Corresponding author (e-mail: shinchberger@eng.uwo.ca).

 doi: 10.1139/T05-082

Fig. 1. Some examples of undrained shear strength versus strain rate for cohesive soils.

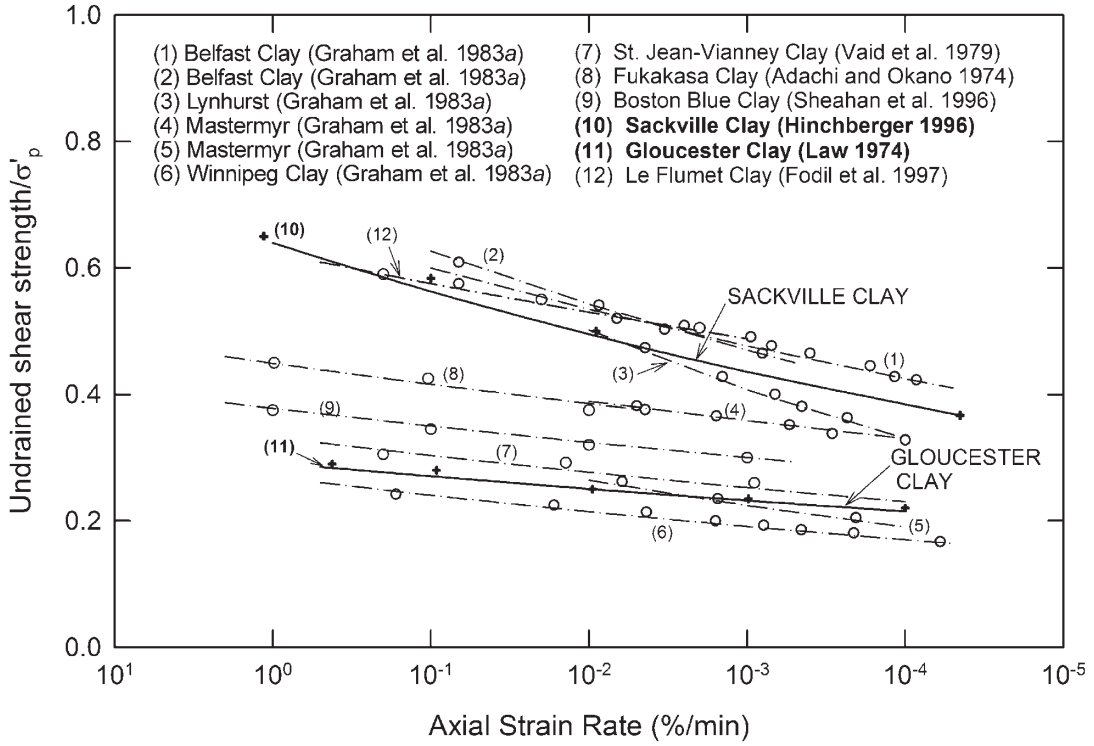

elasticity and classical plasticity. This approach is usually adopted even though many cohesive soils violate some or all of the assumptions implicit in both theories. In some cases, the rate-dependent properties of clay may be neglected and sufficiently accurate predictions obtained. However, there are a number of cases where modeling the rate-sensitive properties of clay is essential for evaluating the performance of embankments built on cohesive foundation soils (e.g., Bozozuk and Leonards 1972; M.I.T. 1975; Rowe et al. 1995; Fodil et al. 1997; Kim and Leroueil 2001).

For some soils, an order of magnitude increase in strain rate results in a 10–20% increase in the measured undrained shear strength (Fig. 1). Considering that field vane and cone penetration tests are undertaken at relatively high strain rates, there is potential for significant error in the measurement of undrained shear strength and subsequent assessment of short-term embankment stability. It is generally recognized that there is a need to develop a constitutive model that can adequately account for strain-rate effects on the engineering properties of soft clay. Accordingly, numerous researchers (e.g., Adachi and Oka 1982; Kavazanjian et al. 1985; Kutter and Sathialingam 1992; Wedage et al. 1998; Hinchberger and Rowe 1998; Kim and Leroueil 2001; Yin et al. 2002; Rocchi et al. 2003) have proposed elastic-viscoplastic formulations to account for the time-dependent behaviour of clay.

In this paper, the predictive ability of two elastic-viscoplastic constitutive formulations is examined using (*i*) the behaviour of Sackville clay during laboratory loading and (*ii*) the laboratory and field response of Gloucester clay (Bozozuk and Leonards 1972; Lo et al. 1976). Both constitutive formulations, one developed by Adachi and Oka (1982) and the other by Rowe and Hinchberger (1998), are three-parameter elastic-viscoplastic models based on stress, strain, and strain rate. Katona and Mulert (1984) and Desai and Zhang (1987) have developed similar three-parameter models for soft rock. The main objectives of this paper are to identify a constitutive formulation that is suitable for use in the study of embankments on soft rate-sensitive clay foundations and to examine the importance of the yield surface function on the constitutive response. In undertaking the present study, the general ability of two three-parameter elastic-viscoplastic constitutive models to describe the effect of strain rate on the engineering behaviour of two soft clays is examined. A new method of evaluating numerical overstress is introduced for elastic-viscoplastic formulations that utilize an elliptical yield surface. The new method of overstress measurement improves the predictive ability of elastic-viscoplastic models based on the elliptical cap yield function (Chen 1982). In this study, it is shown that a single elastic-viscoplastic constitutive framework can account for the effects of strain rate on the engineering response of two natural soft clays subject to both drained and undrained laboratory loading and two-dimensional field loading. Given the range of stress paths and the duration of loading, this evaluation is considered to be unique and of interest to researchers and engineers in this field.

Case histories

Sackville test embankment

In 1989, a geosynthetic reinforced test embankment was built on a soft organic silty clay deposit (CL) in Sackville, New Brunswick, Canada. The embankment performance has been described in detail by Rowe et al. (1995). Rowe et al. (1996) performed a finite element analysis of the test em-

Table 1. Comparison of elastic-viscoplastic models.

Model	Elastic model	Yield function	Failure criterion	Flow function	Hardening law
Original Cam clay (Adachi and Oka 1982)	$K = (1 + e)\sigma'_m/\kappa$, G, ν	$f = \frac{\sqrt{2J_2}}{M\sigma'_m} + \ln(\sigma'_m) - \ln(\sigma'^{(s)}_{my}) = 0$	$f = \sigma'_m M - \sqrt{2J_2} = 0$	$\phi(F) = \gamma^{vp} \exp[n \ln(\sigma'^{(d)}_{my}/\sigma'^{(s)}_{my})]$	$\partial\sigma'^{(s)}_{my} = \frac{(1+e)}{(\lambda-\kappa)}\sigma'^{(s)}_{my}\partial\varepsilon^{vp}_{vol}$
Elliptical cap	$K = (1 + e)\sigma'_m/\kappa$, G, ν	$f = (\sigma'_m - l)^2 - 2J_2R^2 + (\sigma'^{(s)}_{my} - l)^2 = 0$	$f = \sigma'_m M + c'_{NC} - \sqrt{2J_2} = 0$ or $f = \sigma'_m M + c'_{OC} - \sqrt{2J_2} = 0$	$\phi(F) = \gamma^{vp}\left(\frac{\sigma'^{(s)}_{my} + \sigma'^{(d)}_{os}}{\sigma'^{(s)}_{my}}\right)^n - 1$	$\partial\sigma'^{(s)}_{my} = \frac{(1+e)}{(\lambda-\kappa)}\sigma'^{(s)}_{my}\partial\varepsilon^{vp}_{vol}$

bankment using a conventional inviscous modified Cam clay constitutive model (Britto and Gunn 1987) coupled with Biot consolidation theory (Biot 1941) and it was concluded that this approach could not describe the essential features of the embankment behaviour. Rowe and Hinchberger (1998) subsequently performed a finite element analysis of the Sackville case history using an elastic-viscoplastic constitutive model coupled with Biot consolidation theory. This analysis (Rowe and Hinchberger 1998) provided an encouraging description of the embankment behaviour and served to illustrate the importance of considering the effects of strain rate on the engineering response of Sackville clay at yield and failure. In the following sections, the measured response of Sackville clay during undrained and drained laboratory tests is presented and compared with the calculated response obtained using two elastic-viscoplastic constitutive formulations.

Gloucester test embankment

In 1967, the Division of Building Research, National Research Council of Canada, built an unreinforced test embankment at Canadian Forces Station Gloucester, Ontario. Construction of the Gloucester test embankment was undertaken in two stages: the first stage in 1967 (Bozozuk and Leonards 1972) and the second stage in 1982 (Fisher et al. 1982). In addition, several researchers have investigated the behaviour of Gloucester clay during undrained and drained laboratory loading (e.g., Law 1974: Lo et al. 1976; Leroueil et al. 1983). The abundant laboratory and field data made available by this case allow for a thorough evaluation of the elastic-viscoplastic constitutive formulations described below.

Theoretical treatment of strain-rate effects

Constitutive equations

Many cohesive soils exhibit time-dependent stress-strain characteristics at all stress levels. It is, however, generally accepted that the time-dependent behaviour of clay becomes more predominant at stress states that cause yielding and failure in cohesive soils (e.g., Adachi and Oka 1982; Leroueil et al. 1983). For a significant number of cohesive soils, it appears valid to neglect strain-rate effects in the elastic range. Accordingly, this approach was adopted in the present study. Two elastic-viscoplastic yield surface models have been implemented in a finite element program. Both constitutive equations are formulated in terms of mean stress $\sigma'_m = (\sigma'_1 + \sigma'_2 + \sigma'_3)/3$ and the second invariant of the deviatoric stress tensor, J_2. Also, both formulations use the Drucker–Prager failure envelope to define the critical state. Details of the formulations examined are presented below and summarized in Table 1.

Original Cam clay viscoplasticity

The first constitutive formulation is based on the original Cam clay model (Roscoe and Schofield 1963), which was modified by Adachi and Oka (1982) to account for time-dependent plasticity using Perzyna's theory of overstress viscoplasticity (Perzyna 1963). For an elastic-viscoplastic material, the strain rate tensor is:

Fig. 2. Schematic behaviour of the original Cam clay model (Adachi and Oka 1982) during CAU triaxial creep and triaxial compression.

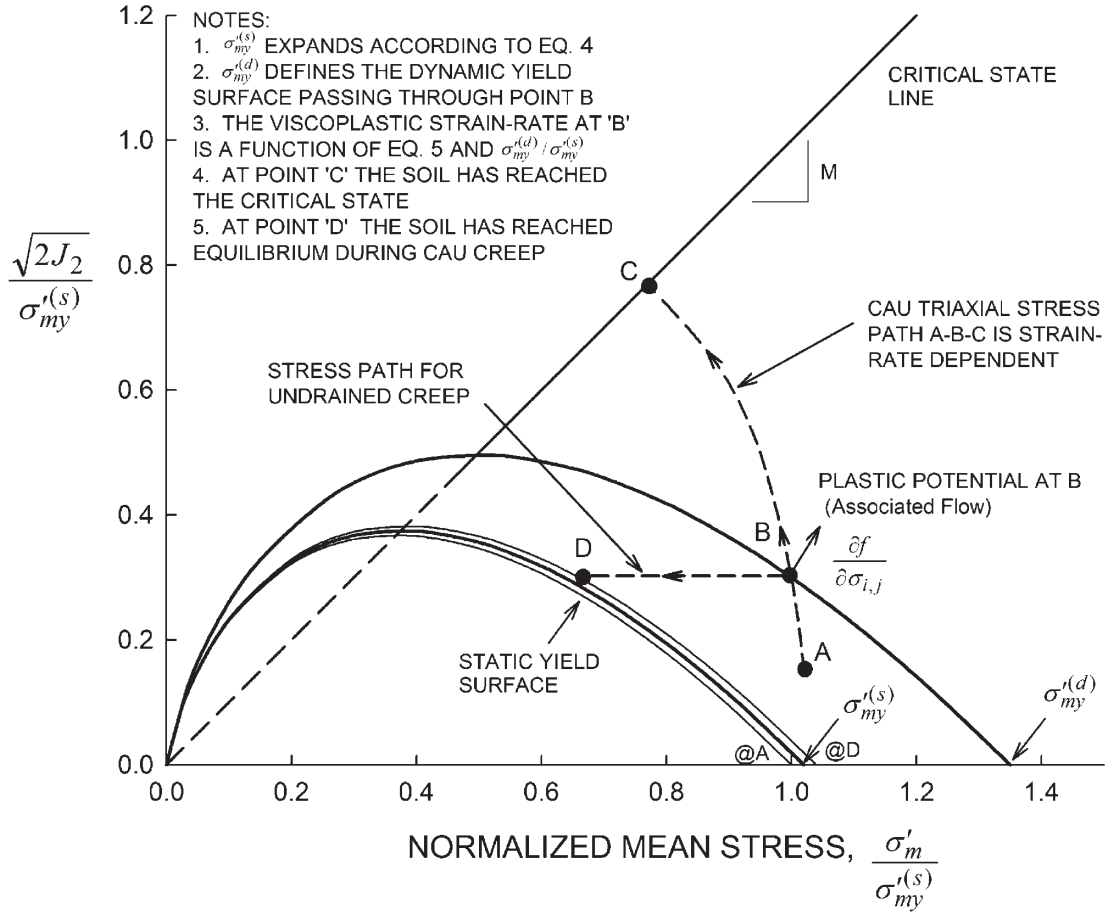

$$[1] \qquad \dot{\varepsilon}_{i,j} = \dot{\varepsilon}^{e}_{i,j} + \dot{\varepsilon}^{vp}_{i,j}$$

where $\dot{\varepsilon}^{e}_{i,j}$ and $\dot{\varepsilon}^{vp}_{i,j}$ are the elastic and viscoplastic strain rate tensors, respectively. In the original Cam clay elastic-visoplastic model, the elastic bulk modulus, K, is assumed to be stress depended viz.

$$[2] \qquad K = \frac{(1+e)\sigma'_m}{\kappa}$$

In eq. [2], κ is the slope of the e – ln (σ'_m) curve in the overconsolidated stress range and e is the void ratio. The dependent shear modulus, G, is related to the bulk modulus by Poisson's ratio, v, as shown in Table 1. Since elastic strains are assumed to be time-independent, $\dot{\varepsilon}^{e}_{i,j}$ in eq. [1] represents the inviscous incremental elastic strain tensor.

In accordance with Perzyna's theory (1963), the viscoplastic strain-rate tensor is defined as follows:

$$[3a] \qquad \dot{\varepsilon}^{vp}_{i,j} = \gamma^{vp} \langle \phi(F) \rangle \frac{\partial g}{\partial \sigma'_{i,j}}$$

where following the convention of overstress viscoplasticity, the notation $\langle\ \rangle$ implies:

$$[3b] \qquad \langle \phi(F) \rangle = \phi(F) \qquad \text{for } F > 0$$

and

$$[3c] \qquad \langle \phi(F) \rangle = 0 \qquad \text{for } F \le 0$$

In eq. [3], γ^{vp} is the fluidity parameter (or inverse of viscosity) with units of inverse time, the scalar function $\phi(F)$ is the flow function, and $\partial g/\partial \sigma'_{i,j}$ is the plastic potential from plasticity theory. The popularity of Perzyna's theory of overstress viscoplasticity is due to its simplicity. The formulation incorporates the yield surface from classical plasticity, and therefore many rate-independent yield surface models (e.g., Roscoe and Burland 1968; Desai et al. 1986; Pastor et al. 1990; Lagioia et al. 1996) can be formulated for viscoplastic material behaviour. The strain-hardening law used in the original Cam clay model is

$$[4] \qquad \partial \sigma'^{(s)}_{my} = \frac{(1+e)}{(\lambda - \kappa)} \sigma'^{(s)}_{my} \partial \varepsilon^{vp}_{vol}$$

where κ and λ are the slopes of the e – ln (σ'_m) curve in the overconsolidated and normally consolidated stress ranges, respectively; $\sigma'^{(s)}_{my}$ is the intercept of the static yield surface with the σ'_m axis; and ε^{vp}_{vol} is the volumetric viscoplastic strain. In tensor form, the constitutive equation is

$$[5] \qquad \dot{\varepsilon}_{i,j} = \frac{\dot{s}_{i,j}}{2G} + \frac{\kappa}{3(1+e)} \frac{\dot{\sigma}'_m}{\sigma'_m} \delta_{i,j} + \gamma^{vp} \langle \phi(F) \rangle \frac{s_{i,j}}{M\sqrt{2J_2}} + \frac{\gamma^{vp} \langle \phi(F) \rangle}{3M} \left(M - \frac{\sqrt{2J_2}}{\sigma'_m} \right) \delta_{i,j}$$

Fig. 3. Schematic behaviour of the elliptical cap model during CAU triaxial creep and triaxial compression.

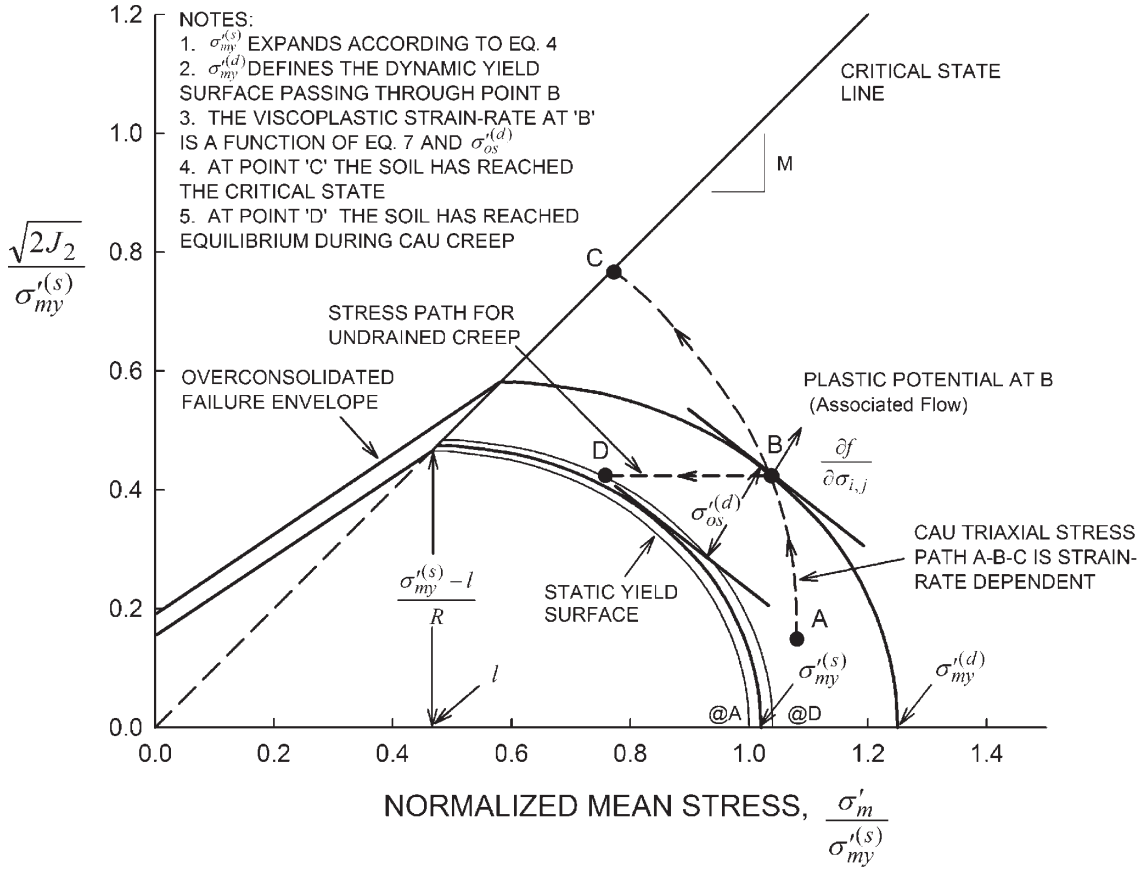

$$\phi(F) = \exp\left[n \ln\left(\frac{\sigma'^{(d)}_{my}}{\sigma'^{(s)}_{my}} \right) \right]$$

where $s_{i,j}$ is the deviatoric stress tensor, J_2 is the second invariant of the deviatoric stress tensor, σ'_m is the mean effective stress, $\delta_{i,j}$ is Kronecker's delta, G is the dependent shear modulus, κ is the slope of the $e - \ln(\sigma'_m)$ curve in the overconsolidated stress range, M is the effective stress ratio at failure, e is the void ratio, γ^{vp} is the fluidity constant, and $\sigma'^{(d)}_{my}/\sigma'^{(s)}_{my}$ is a measure of the overstress. The Adachi and Oka model (1982), referred to as the original Cam clay model for the remainder of this paper, is illustrated in Fig. 2 for a typical undrained stress path considered in this investigation.

Elastic-viscoplastic elliptical cap model

The second constitutive model considered is based on the Drucker–Prager failure envelope and the elliptical cap yield surface (Chen 1982). To facilitate direct comparison of the original Cam clay and the elliptical cap constitutive models, the elastic bulk modulus was assumed to be dependent on the mean stress, σ'_m, according to eq. [2]. Similarly, eq. [4] was assumed to govern strain hardening of the elliptical yield surface. It is recognized that there are many different hardening laws proposed for cohesive soils, however, the intent was to retain most of the critical state concepts (Roscoe and Schofield 1963) in both formulations to allow direct comparison and to limit the number of constitutive modifications introduced. The equation of the elliptical yield surface in $\sqrt{2J_2} - \sigma'_m$ stress space is

$$[6] \qquad f^{(s)} = (\sigma'_m - l)^2 + 2J_2R^2 - (\sigma'^{(s)}_{my} - l)^2 = 0$$

where l, R, and $\sigma'^{(s)}_{my}$ are defined in Fig. 3. The constitutive equation for the elliptical cap model investigated in this paper is

$$[7] \qquad \dot{\varepsilon}_{i,j} = \frac{\dot{s}_{i,j}}{2G} + \frac{\kappa}{3(1+e)} \frac{\dot{\sigma}'_m}{\sigma'_m} \delta_{i,j} + \gamma^{vp} \langle \phi(F) \rangle \left[\frac{\delta_{i,j}}{3} - \left(\frac{2l}{\sigma'^{(d)}_{my}} - 1 \right) \left(\frac{\sigma'^{(d)}_{my}}{\sigma'_m} \right)^2 \frac{\delta_{i,j}}{3} - R \left(\frac{\sqrt{2J_2}}{\sigma'_m} \right)^2 \frac{\delta_{i,j}}{3} + \frac{2s_{i,j}R^2}{\sigma'_m} \right]$$

$$\phi(F) = \left(\frac{\sigma'^{(s)}_{my} + \sigma'^{(d)}_{os}}{\sigma'^{(s)}_{my}} \right)^n - 1$$

where all of the constants in eq. [7] have been defined previously except the parameter $\sigma'^{(d)}_{os}$, which mathematically represents the level of overstress. The parameter $\sigma'^{(d)}_{os}$ will be discussed further in a later section. Comparing eqs. [5] and [7], the flow functions, $\phi(F)$, are essentially equivalent for isotropic compression, and they are mathematically similar for stress paths typically encountered in situ during embank-

ment construction. The elliptical cap yield surface becomes equivalent to the modified Cam clay yield surface for $R = 1/M$ and $l = 0.5\sigma'^{(s)}_{my}$.

In the elliptical cap formulation, the Drucker–Prager failure envelope (eq. [8]) was used to define failure in the overconsolidated stress range,

$$[8] \qquad f^{(s)} = M_{OC}\,\sigma'_m + c'_{OC} - \sqrt{2J_2} = 0$$

where M_{OC} and c'_{OC} are the slope of the failure envelope and the cohesion intercept in the overconsolidated stress range, respectively. The failure envelope in the normally consolidated stress range is also defined using eq. [8] but with the parameters M and c'_{NC}. Fig. 3 illustrates the main elements of this model and a typical strain rate depended stress path during consolidated anisotropic undrained (CAU) triaxial compression.

Hydraulic conductivity relationship

In investigating the constitutive response of Sackville and Gloucester clay, the relationship between hydraulic conductivity and void ratio was assumed to vary as follows (e.g., Tavenas et al. 1983):

$$[9] \qquad k = k_o \exp\,[(e - e_0)/C_k)]$$

where k_o is the hydraulic conductivity at void ratio, e_0, e is the void ratio, and C_k is the slope of the void ratio versus hydraulic conductivity in e – log (k) space. The vertical hydraulic conductivity, k_v, was calculated using eq. [9], and the horizontal hydraulic conductivity, k_H, is given by

$$[10] \qquad R_k = \frac{k_H}{k_v}$$

Although cross-anisotropic permeability has been assumed, the stress–strain behaviour of both formulations is isotropic.

Discussion

A number of researchers have measured the shape of the yield surface for cohesive soils (e.g., Mitchell 1970; Tavenas and Leroueil 1977; Graham et al. 1983*b*). Figure 4 summarizes data for three natural clays. It is evident that the yield surface shape and aspect ratio varies from soil to soil. To further illustrate this point, the elliptical yield surface parameters, R, required to fit yield points for a number of clays reported in the literature, are presented in Table 2. The elliptical cap (eq. [6]) was selected for the present study since it can be scaled through the parameters R and l (Fig. 3) to model the aspect ratio and approximate shape of the Sackville and Gloucester yield surfaces. It is noted, however, that the elliptical cap yield surface fit becomes less acceptable as the structure of the clay increases. Accordingly, eq. [6] may not be appropriate for highly structured or cemented clays, such as Saint-Alban clay (e.g., Tavenas and Leroueil 1977; Leroueil 1997), where the yield surface appears to be rotated about the K'_o–stress axis in stress space. From a practical point of view, however, the elliptical cap yield surface permits scaling to approximately fit the yield surface of soft clay over the predominant stress paths appropriate to embankment loading for soils that are quasi-isotropic and that do not exhibit significant structure. Although two additional constitutive parameters are introduced, the parameters R and l do not require additional testing and can be estimated from standard incremental oedometer and triaxial compression tests.

Fig. 4. The yield surface of three natural clay soils.

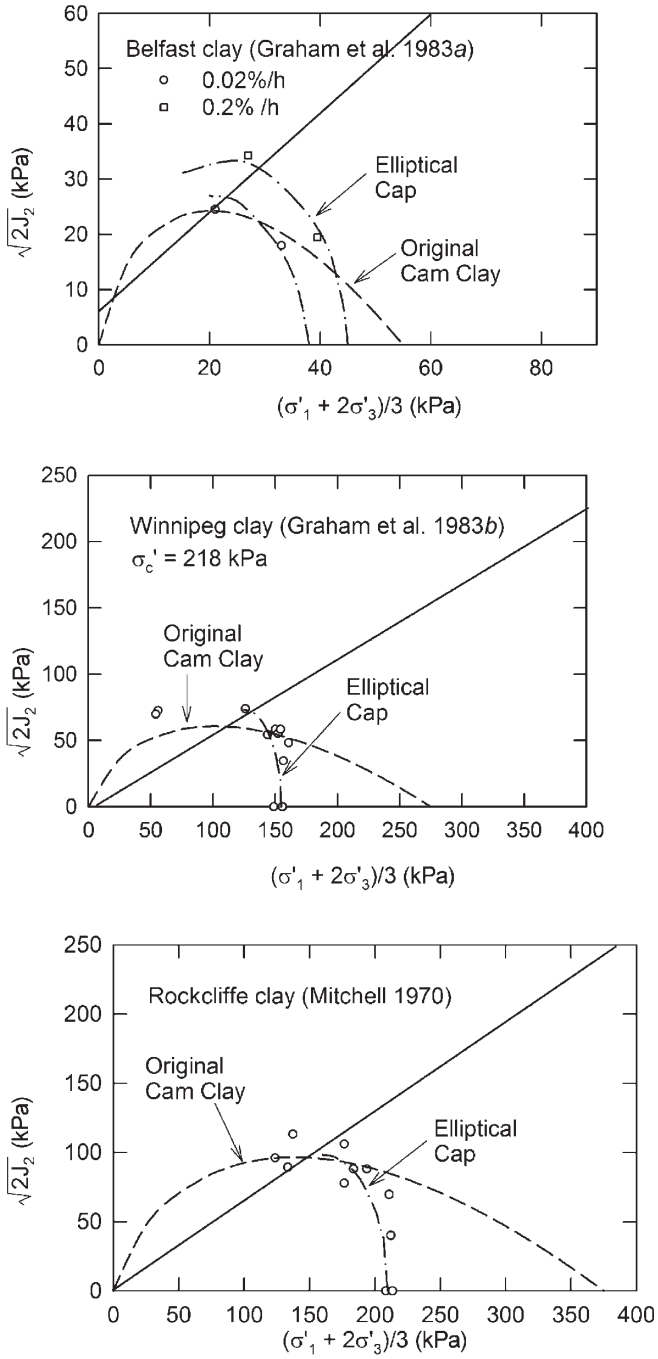

There are a number of similarities between the original Cam clay and the elliptical cap models adopted herein that permit direct comparison and evaluation. Specifically, both formulations use (*i*) the same elastic model, (*ii*) the same strain-hardening law, (*iii*) an associated flow rule, and (*iv*) a similar overstress function based on the power law (Norton 1929). Accordingly, for stress states that cause yielding and failure of clayey soils, the overstress response of both models is similar.

Table 2. Variability of the yield surface cap aspect: loading stress paths.

Soil	Aspect ratio*, R	Failure envelope parameter		Reference
		M	c' (kPa)	
Gloucester clay	1.65	0.9	0	This paper
Sackville clay	1.1–1.2	0.96–1.06	18.0	This paper
Sarnia clay	1.5–2.0	0.9	0.0	Dittrich 2002
Rockcliffe clay	0.55	0.65	0	Mitchell 1970
Belfast clay	0.65	0.9	8.0	Graham et al. 1983*a*
Winnipeg clay	0.4	0.61	0	Graham et al. 1983*b*

*In $\sqrt{2J_2} - \sigma'_m$ stress space.

Table 3. Laboratory test on Sackville clay.

Test No.	Depth (m)	w_N	w_P	w_L	Cell pressure (kPa)	Strain rate (%/min)	Deviator stress (kPa)
CAU*-1	3.65–3.85	57.0	31.0	50.1	56	0.009	—
CAU-2					56	0.10	—
CAU-3					56	1.14	—
CAU-4	2.3–2.5	41.5	29.0	42.1	47	0.012	—
CAU-5					47	1.14	—
CAU-6	6.65–6.85	45.4	31.6	48.5	56	0.012	—
CAU-7					56	1.14	—
CAU-8	5.5–5.7	102.5	34.5	82.1	56	0.009	—
CAU-9					56	0.10	—
CAU-10					56	1.14	—
CAUCr†-11	5.5–5.7	82.7	50.6	82.0	56	—	28.0, 34.5
CAUCr-12	2.3–2.5	43.3	28.9	42.0	47	—	28.0, 42.0
CAUCr-13	6.65–6.85	44.0	33.2	48.5	56	—	35, 44.5, 50.0
CAUCr-14	3.65–3.85	45.7	30.1	49.1	56	—	34.5–40.5

*Anisotropically consolidated undrained compression ($K'_o = 0.76$).
†Anisotropically consolidated undrained creep ($K'_o = 0.76$).

There are, however, two significant differences between the formulations. First, the aspect ratio of the original Cam clay yield surface cannot be varied without adjusting the critical state parameter, M. The elliptical cap is more flexible in this regard and can be varied through the parameters, R and l, to obtain almost any ratio of undrained shear strength, c_u, to preconsolidation pressure, σ'_p. This can be done without altering the critical state parameter, M. The original Cam clay yield surface cannot fit the yield loci of most natural soft clays shown in Fig. 4. Thus, it is necessary to investigate the implications of adopting the original Cam clay yield surface for elastic-viscoplastic constitutive modelling.

The second significant difference is the mathematical method of evaluating overstress. In the viscoplastic original Cam clay model (Adachi and Oka 1982), the level of overstress is defined by the ratio of dynamic yield surface intercept and the static yield surface intercept, $\sigma'^{(d)}_{my}/\sigma'^{(s)}_{my}$ (see Fig. 2). In the elliptical cap formulation proposed herein, overstress $\sigma'^{(d)}_{os}$ is evaluated by method of parallel yield surface tangents, which is a significant modification to conventional elastic-viscoplastic formulations. For reasons of mathematic convenience, it is common to use the yield surface function to measure overstress (e.g., Adachi and Oka 1982; Katona and Mulert 1984; Desai and Zhang 1987). Thus, for stress states that exceed static yield, a dynamic yield surface $f^{(d)}$ is defined passing through the current state of stress (point B in Figs. 2 and 3) with intercept, $\sigma'^{(d)}_{my}$. Overstress is then taken as the ratio $\sigma'^{(d)}_{my}/\sigma'^{(s)}_{my}$ or $f^{(d)}/f^{(s)}$ (Fig. 2) and the rate of viscoplastic strain is taken to be proportional to the overstress ratio. In this study, a new method of overstress measurement for elliptical yield surfaces has been used. The method of evaluating overstress utilizes parallel yield surface tangents, and the resultant modifications enable the elliptical cap formulation to predict apparent yield surface expansion in stress space due to strain-rate effects that is more consistent with experimental observations. For example, Graham et al. (1983*a*) have shown that the yield surface of Belfast clay appears to expand almost uniformly in $\sqrt{2J_2} - \sigma'_m$ stress space because of increases in strain rate (see Fig. 4). Fukukasa clay (Adachi and Oka 1982), Sackville clay, and Gloucester clay (Hinchberger 1996) appear to exhibit similar behaviour, which can be approximated by the overstress measurement illustrated in Fig. 3. Without this modification, the strain-rate dependent stress path of the elliptical cap model (Fig. 3) is highly nonlinear (e.g., Kutter and Sathialingam 1992) and does not provide a good description of the measured strain-rate dependent stress path for the clays considered here.

The preceding discussions provide some background into the elastic-viscoplastic formulations evaluated in this paper. These two constitutive models were implemented in the finite element program AFENA (Carter and Balaam 1995) to

identify a constitutive formulation that can satisfactorily describe the time-dependent response of embankments on soft rate-sensitive clay foundations. Complete details of the finite element implementation of eqs. [5] and [7] are described elsewhere (e.g., Oka et al. 1986; Hinchberger 1996).

Laboratory investigations

Sackville clay

For Sackville clay, strain-rate dependency was studied using a series of relatively conventional undrained and drained laboratory tests, which are summarized in Table 3. Anisotropically consolidated undrained triaxial compression tests (CAU) were performed using standard 50 mm diameter and 100 mm long samples. The axial strain rates ranged from 0.009%/min to 1.14%/min. In addition, CAU triaxial creep tests were performed at deviator stresses that varied from 28 kPa to 50 kPa. All laboratory tests were performed at room temperature except CAU undrained creep tests, which were conducted in an environmental room at a relatively constant temperature of 10.5 ± 0.5 °C. A typical CAU creep test involved two to three stages. The procedure used in testing Sackville soil from a depth of 5.6 m is described in the following section to illustrate the test methodology.

First, the soil was trimmed, placed in a triaxial cell (with membrane), saturated, and then anisotropically consolidated for 24 h. Next, the drainage valves were closed and the deviator stress was increased to 35 kPa and maintained for about 8000 min until the axial strains and excess pore pressure stabilized. In the second stage, the deviator stress was increased to 44.5 kPa and maintained until axial deformations and excess pore pressures stabilized (12 000 min). In the final test stage, the deviator stress was increased to 50 kPa and maintained for about 12 000 min. In all but the last creep stage, the deviator stress was maintained until the stress state reached equilibrium and the axial strain rate became insignificant. In the last creep stage, although the excess pore pressures generally stabilized, the applied deviator stress produced a constant rate of axial strain (or constant creep rate). As discussed below, the final equilibrium stress states measured during long-term CAU triaxial creep tests were used to estimate the initial yield surface intercept, $\sigma'^{(s)}_{my}$, and the cap parameters R and l.

For each CAU triaxial compression test, the first phase involved consolidating the soil to a mean stress approximately 20% higher than the estimated in situ mean stress. Consequently, there was secondary compression at the end of each 24 h consolidation stage, which was taken into account during modeling by adopting an initial state of overstress (see Figs. 2 and 3). The intent of the laboratory investigation was to study the time-dependent plastic flow of Sackville clay, and consequently, consolidation stresses above the mean in situ stress were chosen to ensure plastic response. In taking this approach, consideration was given to the impact of the test procedure on the initial fabric or structure of Sackville clay. In general, Sackville clay did not exhibit evidence of significant structure. Gnanendran (1993) found that the shear strength of Sackville clay was essentially isotropic and the behaviour during triaxial compression could be classified as strain hardening. A typical oedometer curve is shown in Fig. 5, which shows a linear compression response in the overconsolidated range, a poorly defined preconsolidation pressure followed by essentially linear virgin compression in e – log σ'_v space. The calculated and measured behaviour during incremental oedometer consolidation are also considered in the following constitutive evaluation.

Fig. 5. Oedometer and triaxial consolidation curves for Sackville clay from depths of 3.8 m and 6.8 m.

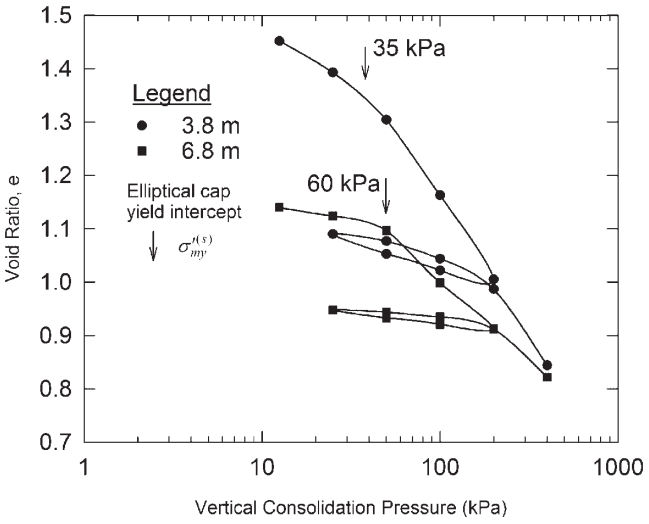

Gloucester clay

Lo et al. (1976) describe the results of long-term consolidation tests conducted on specimens trimmed from Oesterberg samples and Block samples retrieved from the Gloucester site. The load increment applied in the long-term tests corresponded to the calculated load increment in the field caused by construction of the test embankment. The following specimen sizes were considered: (*i*) conventional 5.08 cm diameter by 1.27 cm thick samples tested in a fixed ring oedometer apparatus, (*ii*) 11.28 cm diameter and 5.08 cm thick specimens trimmed from Oesterberg samples and tested in a modified Rowe cell apparatus, and (*iii*) 15.24 cm diameter and 5.08 cm thick specimens trimmed from block samples and tested in a Rowe cell with pore pressure measurement (Lo et al. 1976). The long-term tests were conducted for durations of up to 150 days and the axial strain and excess pore pressure data is used in the present evaluation. It is noted that some uncertainty is introduced in the use of one-dimensional consolidation data to assess two-dimensional constitutive models since the confining stress during the test is not measured.

Evaluation

Selection of constitutive parameters

The elastic and viscoplastic material constants used to obtain the calculated behaviour of Sackville clay are summarized in Table 4. In general, the selection of constitutive parameters for both elastic-viscoplastic formulations (eqs. [5] and [7]) involved an iterative process that can be characterized by the following steps:

(*i*) Conventional oedometer consolidation tests were performed to measure the preconsolidation pressure of Sackville clay and to estimate the constitutive parame-

Table 4. Summary of constitutive parameters: Sackville clay.

			Original Cam clay model			Elliptical cap model				
Depth (m)	κ*	λ*	M (ϕ')	γ^{vp} (s^{-1})	n	γ^{vp} (s^{-1})	n	R	c'_{NC}/c' (kPa)	M (ϕ')
3.8	0.04	0.23	1.49 (42°)	5×10^{-9}	20	5×10^{-9}	20	1.2	11/6	1.03 (30.5°)
5.6	0.06	0.28	1.49 (42°)	5×10^{-9}	15.5	5×10^{-9}	20	1.1	18/11	1.03 (30.5°)
6.8	0.03	0.15	1.49 (42°)	8.6×10^{-10}	26	1.1×10^{-9}	30	1.2	18/11	0.96 (28.0°)

*Parameters common to both models.

Fig. 6. Calculated and measured axial strain during CAU triaxial creep tests on Sackville clay from 5.6 m.

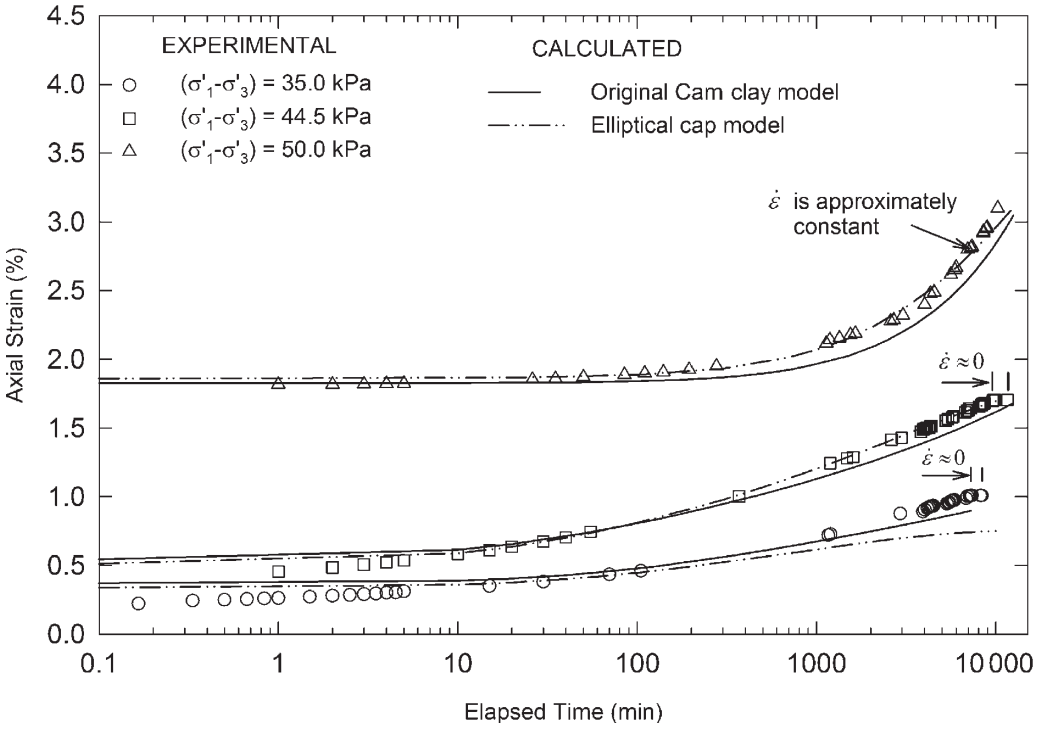

ters, κ and λ, for use in the analysis. Poisson's ratio, v, was assumed to be 0.3.

(*ii*) Failure envelope parameters, c'_{NC} and M, were selected based on the stress states at failure measured in CAU triaxial compression tests.

(*iii*) For the elliptical cap model, equilibrium stress states during CAU triaxial creep were used to determine the cap parameters R, l, and $\sigma'^{(s)}_{my}$. These parameters, in conjunction with eq. [4], define a locus of stress states associated with zero strain rate (or zero creep rate). For the original Cam clay model, only the static yield surface intercept, $\sigma'^{(s)}_{my}$, could be varied to fit the actual equilibrium states.

(*iv*) An estimate of the viscoplastic constitutive parameters, γ^{vp} and n, was obtained by fitting CAU triaxial compression data.

(*v*) The fluidity parameter, γ^{vp}, was then adjusted to optimize agreement between calculated and measured response during CAU triaxial creep tests.

(*vi*) Further adjustments were made to R and l to retain agreement with both CAU triaxial creep and triaxial compression data.

It is generally accepted that temperature can have a significant impact on the viscous response of clay during creep tests. In this study, however, temperature effects did not have a major impact on the constitutive parameters required to fit the test data. This is attributed to the calibration procedure where γ^{vp} was adjusted to fit creep rates during CAU triaxial creep tests conducted at 10.5 °C. It is also attributed to the strain-rate parameter, n, (see $\phi(F)$ in eqs. [5] and [7]), which dominates the theoretical response of the model during CAU triaxial compression.

Sackville clay: CAU triaxial creep

As noted in Table 3, multistage CAU triaxial creep tests were conducted on soil samples retrieved from depths of 2.4 m, 3.8 m, 5.6 m, and 6.8 m, respectively. Axial strain is plotted versus time in Fig. 6 for soil from a depth of 5.6 m. The measured excess pore pressure versus time is plotted in Fig. 7. Calculated behaviour is also plotted in Figs. 6 and 7 for both original Cam clay and elliptical cap constitutive formulations.

Based on Figs. 6 and 7, it can be seen that the overall trend of axial strain and excess pore pressure measured during CAU triaxial creep are adequately described by both the elliptical cap and original Cam clay formulations. Both constitutive models overestimate the initial axial deformations in the early stages of each creep increment. Similar observa-

Fig. 7. Calculated and measured excess pore pressure during CAU triaxial creep tests on Sackville clay from 5.6 m.

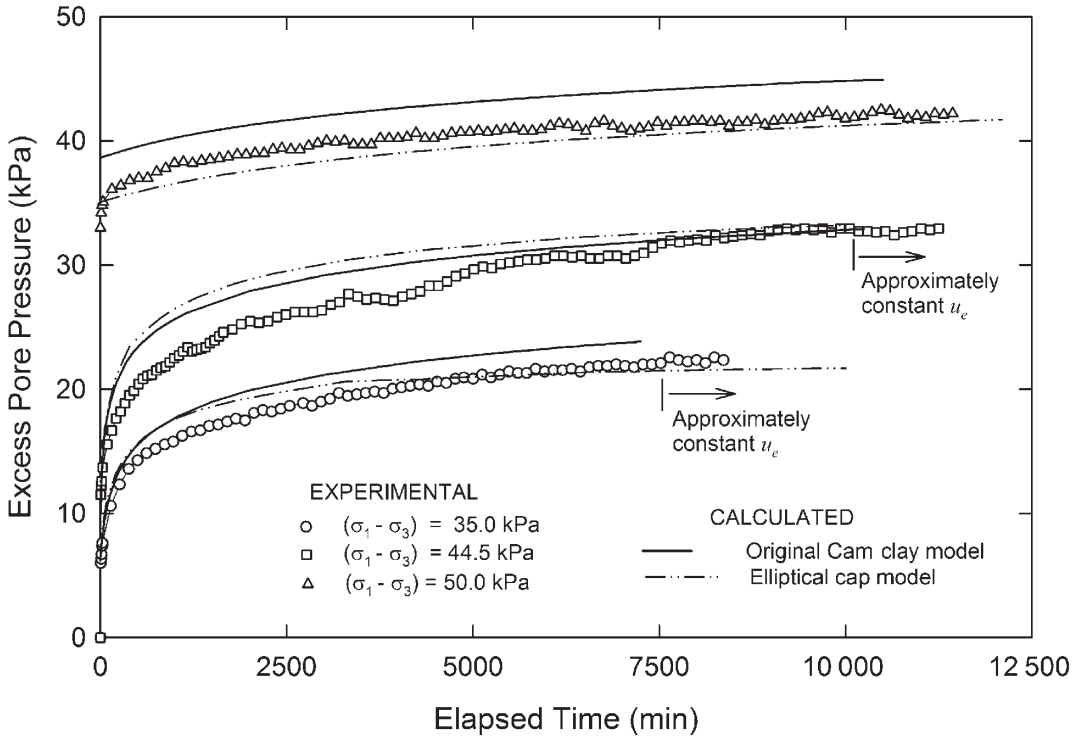

tions were made for Sackville clay from depths of 2.4 m, 3.8 m, and 6.8 m (Hinchberger 1996). In most cases, however, agreement between measured and calculated axial strain becomes satisfactory about 8–10 min after application of each deviator stress increment (see Fig. 6). From a practical point of view, the difference between measured and calculated behaviour is considered to be acceptable and can be attributed to idealizations introduced in both formulations (e.g., a power-law flow function, assumption of associated flow and isotropy, the assumed yield surface equations, etc.).

Sackville clay: CAU triaxial compression

Figures 8 and 9 compare measured and calculated stress paths during CAU triaxial compression tests on Sackville clay from 5.6 m depth. Equilibrium stress states measured during multistage CAU triaxial creep tests are also plotted in Figs. 8 and 9. As described above, the equilibrium stresses measured during CAU triaxial creep were used to estimate the initial yield surface intercept, $\sigma_{my}^{(s)}$, and the aspect ratio, R = 1.10, of the elliptical cap yield surface. The theoretical equilibrium surface is also shown in Figs. 8 and 9 for each constitutive formulation.

Overall, both original Cam clay and elliptical cap formulations are able to satisfactorily describe the effect of strain rate on the stress path and undrained shear strength of Sackville clay. Both constitutive models tend to underestimate the excess pore pressure at low deviator stresses and overestimate the excess pore pressures at higher levels of deviator stress. The critical state parameters adopted in the elliptical cap and original Cam clay formulations are listed in Table 4. For the elliptical cap model, satisfactory agreement with measured response during CAU triaxial compression could be obtained for critical state parameters equivalent to c' = 10 kPa and ϕ' = 30°. Failure envelope parameters c' = 10 kPa and ϕ' = 30° were measured by Gnanendran (1993) for Sackville clay using both CAU and consolidated isotropically drained (CID) triaxial compression tests. In the case of the original Cam clay formulation, a critical state parameter, M, of 1.49 (ϕ' = 42°) was required to obtain similar agreement with measured behaviour. The relatively high critical state parameter, M, is outside the range of typical values for soft silty clay and serves to illustrate one of the limitations of the original Cam clay model. Specifically, the original Cam clay yield surface is not flexible enough to simultaneously fit points on the Sackville yield surface and the failure envelope of Sackville clay.

The deviator stress versus strain response for Sackville clay from a depth of 5.6 m is presented in Fig. 10 and compared with calculated behaviour. Both models can simulate the effect of strain rate on the material stiffness and undrained shear strength. Better agreement between measured response and calculated response is obtained using the elliptical cap formulation; however, both constitutive models are considered to provide an adequate description of soil behaviour. For the elliptical cap formulation, the improved agreement between calculated and measured deviator stress versus axial strain is attributed to the yield surface shape and the resultant plastic potential. In addition, the elliptical cap model is sufficiently flexible to permit selection of failure envelope parameters, c' and M, and cap parameters, R and l, to fit the test data. Such adjustments could not be made with the original Cam clay model.

Sackville clay: conventional incremental oedometer consolidation

Calculated and measured axial strain is plotted versus log time in Fig. 11 for an oedometer increment of 50–100 kPa

Fig. 8. Calculated and measured stress path during CAU triaxial compression on Sackville clay from 5.6 m: original Cam clay model.

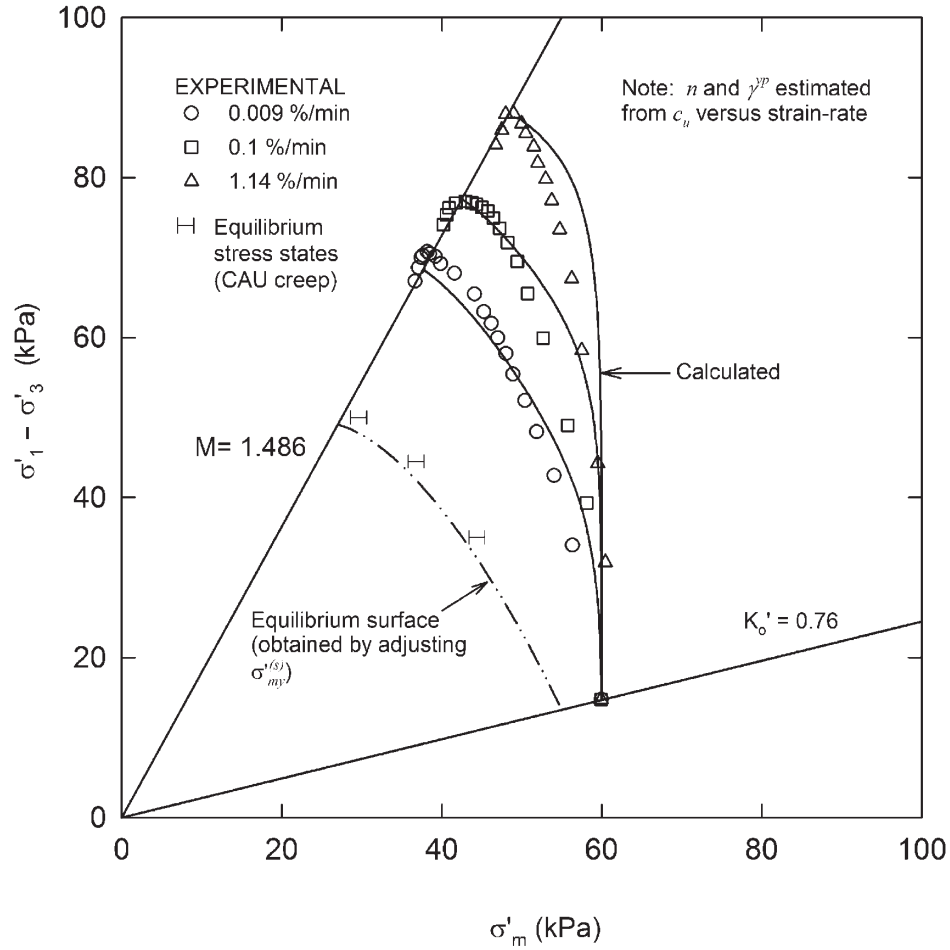

on soil from a depth of 3.8 m. The consolidation test was modeled using the finite element program AFENA with cubic strain triangles, assuming axisymmetric geometry, two-way drainage, and neglecting friction at the top and bottom of the sample. The decrease in hydraulic conductivity of Sackville soil was described using eq. [9] and a complete list of soil parameters used in the analysis is summarized in Table 4 and Fig. 11. It is significant to note that the viscosity parameters (n and γ^{vp}) estimated from CAU triaxial compression tests were used in the consolidation calculations.

There is good agreement between measured and calculated behaviour during virgin oedometer compression. For the elliptical cap model, the calculated rate of secondary compression agrees more closely with the measured rate of secondary compression. Furthermore, a good fit between calculated and measured axial strain is obtained for a yield surface intercept of 35 kPa (see Fig. 5) suggesting that yielding occurred during the stress increment 25–50 kPa. This is in agreement with conventional interpretations of e – log σ_v data. In the numerical computations, the mathematical level of overstress builds during the 25–50 kPa stress increment reaching equilibrium with the mobilized effective strain rate for subsequent stress increments. The mobilized effective strain rate depends on the compressibility of the clay, the hydraulic conductivity, and the duration of the load increments: in this case 24 h. Numerically, the build-up of overstress during the 25–50 kPa stress increment causes the preconsolidation pressure to be poorly defined. For stress increments above 100 kPa, Hinchberger (1996) showed that the calculated axial strain versus log time is independent of the initial yield surface intercept (e.g., $\sigma'^{(s)}_{my}$ = 30 kPa or 35 kPa). The original Cam clay model was found to generally overestimate the rate of secondary compression, although the agreement could have been improved with minor adjustments to the viscoplastic parameter, n. It is implicit in both the original Cam clay and the elliptical cap formulations that secondary compression is neglected for oedometer increments below the preconsolidation pressure. Accordingly, the models cannot be expected to describe the variation of parameters such as C_α/C_c for all stress increments.

In summary, both constitutive formulations evaluated in the present study were found to satisfactorily describe the rate-dependent response of Sackville clay during CAU triaxial compression, CAU triaxial creep, and conventional incremental oedometer tests. Rowe and Hinchberger (1998) have demonstrated the ability of the elastic-viscoplastic elliptical cap formulation to model the Sackville embankment. It is significant that the viscoplastic parameters obtained from undrained laboratory tests on Sackville clay are also suitable for estimating the rate of secondary compression during drained incremental oedometer tests on standard sample sizes. In the preceding discussions and comparisons, the limitations of the original Cam clay model have been assessed. Specifically, the yield surface equation (see Table 1)

Fig. 9. Calculated and measured stress path during CAU triaxial compression on Sackville clay from 5.6 m: elliptical cap model.

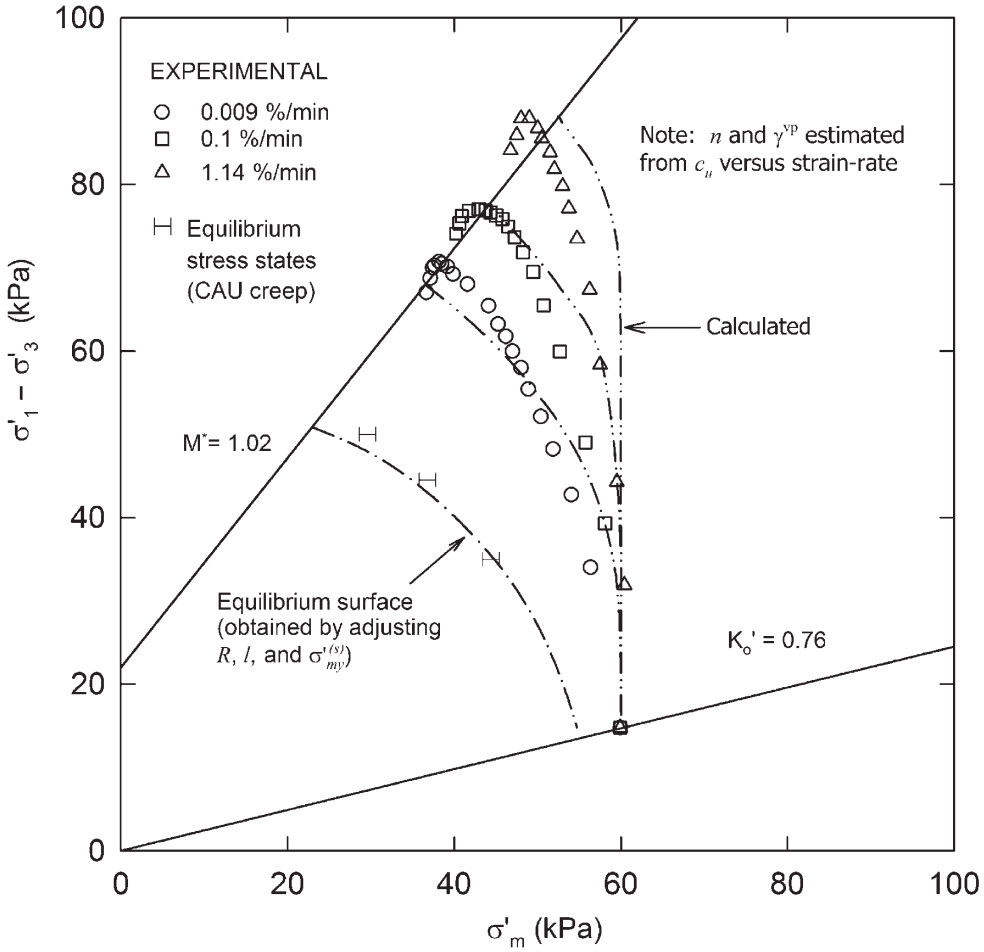

is not flexible enough to describe the engineering response of Sackville clay using failure envelope parameters measured in standard laboratory tests. In the following, both formulations are evaluated using the Gloucester case history.

Gloucester clay: long-term Rowe cell consolidation

Calculated and measured behaviour of Gloucester clay during the long-term Rowe cell consolidation tests are compared in Fig. 12. Constitutive parameters used in the evaluation are summarized in Table 5 for both elliptical cap and original Cam clay elastic-viscoplastic constitutive models. The following is a brief description of the methodology used to obtain the constitutive parameters. A more complete description can be found in Hinchberger and Rowe (1998) and Hinchberger (1996).

The aspect ratio, R = 1.65, of the elliptical cap yield surface was estimated from the ratio of undrained shear strength ($\dot{\varepsilon}_{axial}$ = 0.001%/min) to preconsolidation pressure (measured in incremental oedometer consolidation) for soil from a depth of 2.4 m. For this calculation, K'_o assumed to be 0.8 (see Hinchberger and Rowe 1998). The critical state parameter, M = 0.9, was determined by Law (1974) using a combination of triaxial compression tests with pore pressure measurement. The critical state line does not have a cohesion intercept, (e.g., $c'_{NC=0}$). The hydraulic conductivity parameters and visoplastic constants, n and γ^{vp}, were estimated from long-term consolidation tests undertaken on clay samples from depths of 2.4 m and 4.2 m, as discussed below.

Long-term consolidation tests were modeled using cubic strain triangles, assuming axisymmetric geometry, and neglecting friction at the top and bottom of the sample. One-way drainage was assumed in accordance with the test conditions and the decrease in hydraulic conductivity of Gloucester clay was defined using eq. [9]. Lo et al. (1976) measured the excess pore pressure during Rowe cell consolidation tests and reported the time required for full dissipation of excess pore pressure (see Fig. 12) and 90% dissipation. As a result, the parameters C_k, k_o, and e_o (Table 5) governing hydraulic conductivity and pore pressure dissipation were chosen with a relatively high level of confidence to fit the observed pore pressure dissipation. The strain-rate parameter, n, in eqs. [5] and [7] defines the rate of secondary compression. Accordingly, this parameter was established for both formulations by trial and error until the calculated and measured rates of secondary compression agreed. The yield surface intercept, $\sigma'^{(s)}_{my}$, defines the point of maximum curvature in the axial strain versus log time response (see Fig. 12). The fluidity parameter, γ^{vp}, governs the duration of creep. Accordingly, the fluidity parameter, γ^{vp}, was varied in conjunction with the yield surface intercept,

Fig. 10. Calculated and measured deviator stress versus axial strain during CAU triaxial compression on Sackville clay from 5.6 m.

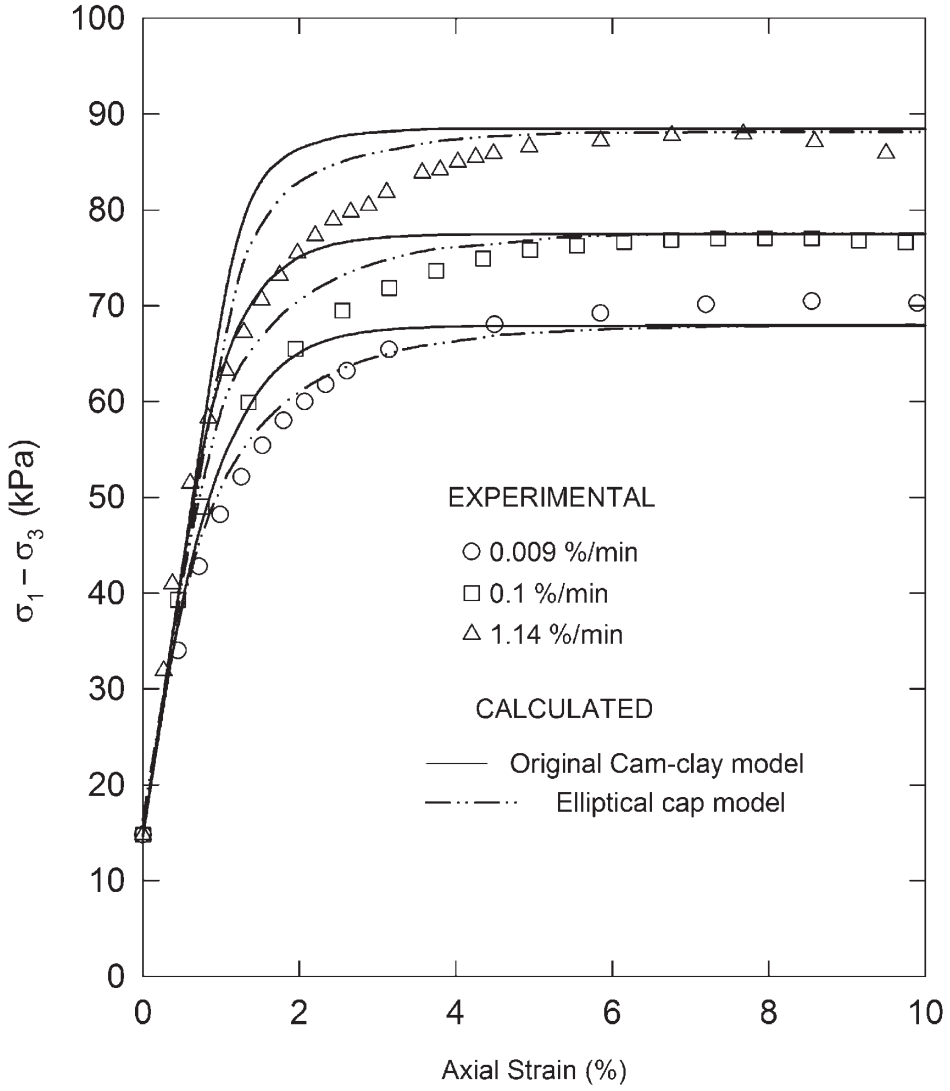

Table 5. Constitutive parameters: long-term Rowe cell consolidation simulations.

	Viscoplastic parameters							
Model	γ^{vp} (s^{-1})	n	e_o	k_o (m/min)	C_k	κ	λ	$\sigma'^{(s)}_{my}$ (kPa)
Original Cam clay	1.7×10^{-10}	28	1.8	1.5×10^{-8}	0.25	0.025	0.65	53*, 58†
Elliptical cap	1.7×10^{-10}	30	1.8	1.5×10^{-8}	0.25	0.025	0.65	48.5*, 56†

*2.4 m depth.
†4.3 m depth.

$\sigma'^{(s)}_{my}$, until an acceptable match between measured and calculated response was obtained.

Figure 12 illustrates the ability of both elastic-viscoplastic yield surface models to simulate the secondary compression response of Gloucester soil during long-term Rowe cell consolidation tests. Both original Cam clay and elliptical cap models were found to adequately describe the dissipation of excess pore pressure and the resultant compression during primary consolidation. In addition, reasonable agreement is observed between the calculated and measured rate of secondary compression after completion of primary consolidation. The elliptical cap model was found to underestimate deformation during primary consolidation for soil from both 2.4 m and 4.3 m depth. For comparison purposes, identical hydraulic conductivity and elastic parameters were used in both formulations.

In summary, both original Cam clay and elliptical cap formulations are able to describe the response of Gloucester clay during long-term Rowe cell consolidation tests. However, the yield surface of most natural clays is approximately elliptical (see Fig. 4). The original Cam clay yield surface is not elliptical. In addition, the aspect ratio of the original Cam clay yield surface is determined by the critical state parameter, M. In contrast, the aspect ratio of the elliptical cap

Fig. 11. Comparison of calculated and measured behaviour during incremental oedometer consolidation on Sackville clay from 3.8 m.

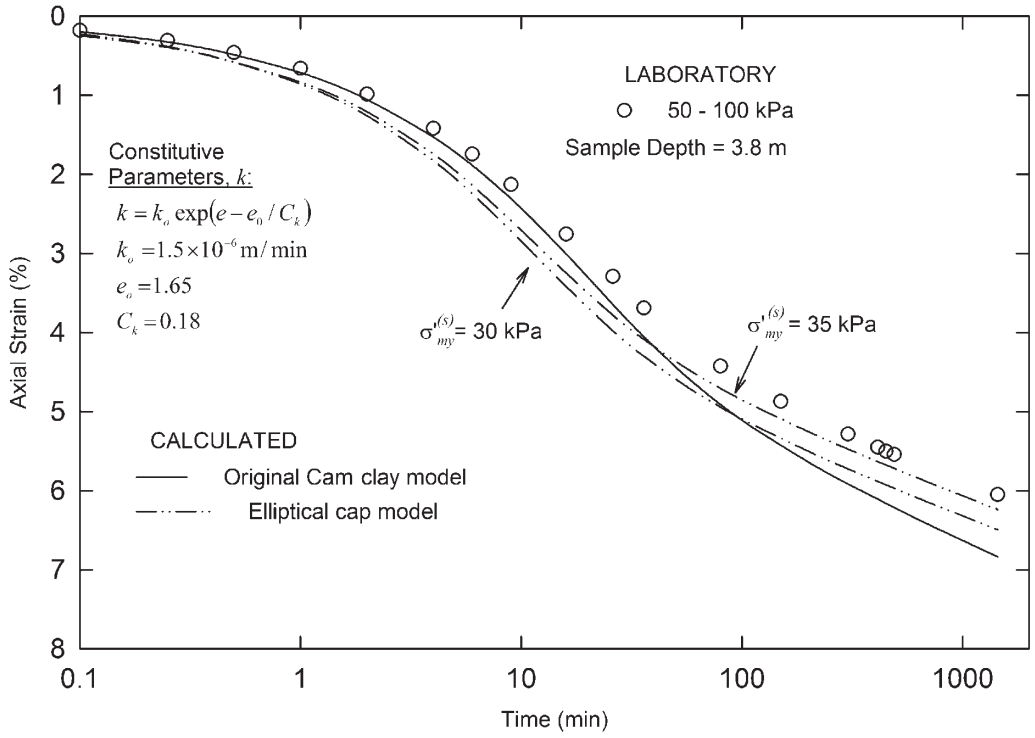

Fig. 12. Comparison of calculated and measured axial strain during long-term Rowe cell consolidation on Gloucester clay.

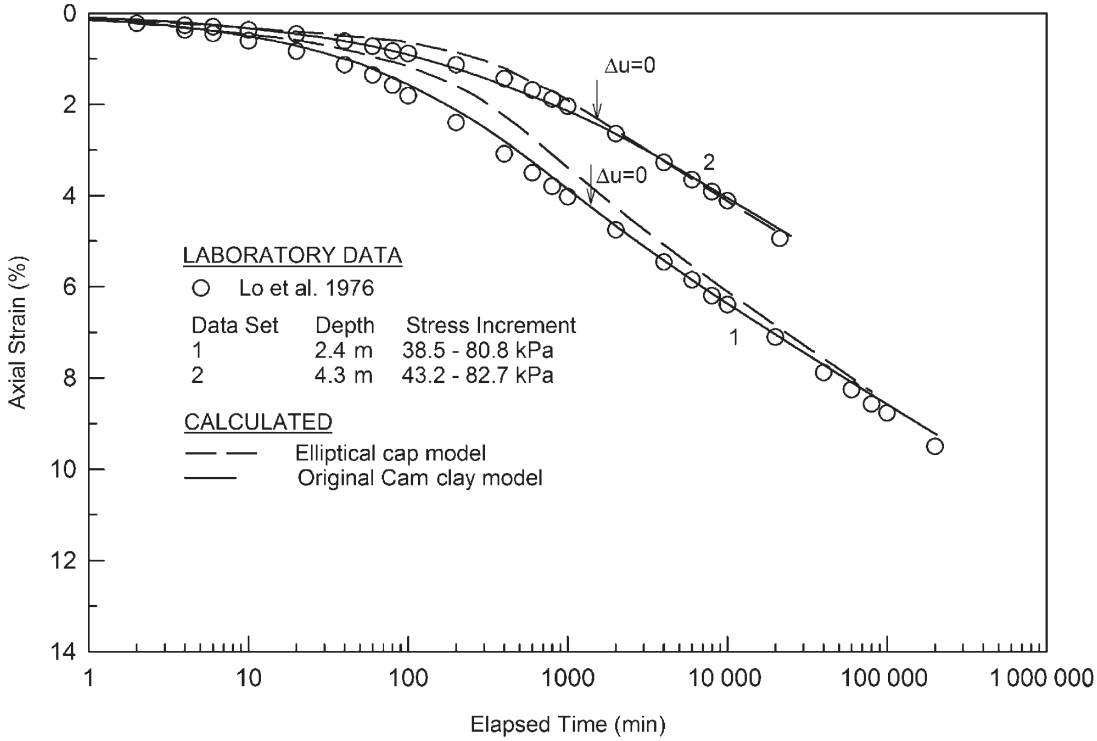

yield surface can be varied to describe the behaviour of Gloucester clay during both long-term oedometer and conventional undrained triaxial compression tests (e.g., Hinchberger 1996; and Hinchberger and Rowe 1998). For Sackville clay, the constitutive limitations of the original Cam clay model were evident from comparison of measured and calculated behaviour during laboratory tests. For Gloucester clay, however, it is not clear how the different yield surface assumptions affect the predictive ability of each constitutive model. Accordingly, the field performance of the Gloucester test embankment is studied to complete the evaluation.

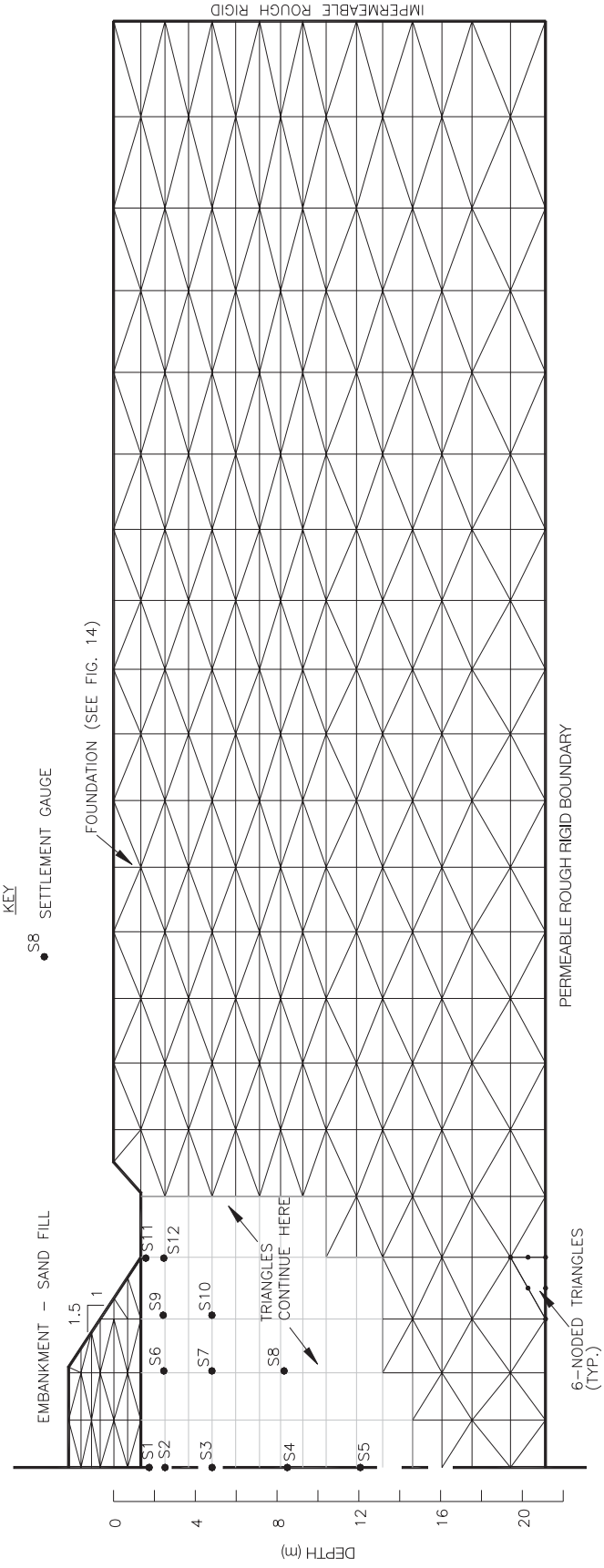

Fig. 13. Finite element mesh and geometry of the Gloucester test embankment.

Field performance: Gloucester test embankment

In 1967, a test embankment was built and instrumented at Gloucester, Ontario. The embankment was composed of granular fill of height 3.7 m constructed in a 1.2 m deep excavation. The crest width of the embankment was 9.2 m and the side slopes were built with a gradient of 1.5 horizontal to 1 vertical. Figure 13 shows the finite element mesh used to model the Gloucester test fill in addition to some details of the test embankment geometry, foundation depth, and instrumentation. Figure 14 provides a summary of the subsurface conditions. Additional details of the Gloucester case history are given by Bozozuk and Leonards (1972), Lo et al. (1976), Tavenas et al. (1983), and Hinchberger and Rowe (1998).

In this study, the Gloucester foundation was discretized to a depth of 20.2 m using six-noded linear strain triangles (see Fig. 13). At 20.2 m depth, a rough rigid permeable boundary was assumed. The foundation soil was modeled as an elastic-viscoplastic material coupled with Biot consolidation theory. Plane strain conditions were assumed and both original Cam clay and elliptical cap formulations were considered in the analysis. The embankment fill (sand fill) was modeled as an inviscous elastoplastic material with a Mohr–Coulomb failure criterion and flow rule of the form proposed by Davis (1968). The Young's modulus of the fill was assumed to be dependent on the minor principle stress by Janbu's equation (Janbu 1963).

Table 6 provides a summary of the constitutive parameters utilized in this study. In addition, Fig. 14 shows the distribution with depth of constitutive parameters such as the vertical hydraulic conductivity, yield surface intercept, and compression index. In summary, the constitutive parameters were chosen based on extensive laboratory and in situ test data. As shown in Fig. 14, there is close agreement between measured and assumed parameters. For comparison purposes, identical constitutive parameters were used for the original Cam clay and elliptical cap formulations. Only the yield surface shape and the yield surface intercept differed. Referring to Fig. 14, in both models the yield surface intercept was assumed to vary with depth similar to the vertical preconsolidation pressure. For all depths, the assumed yield surface intercept for the original Cam clay analysis is higher than that of the elliptical cap based on analysis of long-term oedometer creep tests (see Fig. 12 and Table 5). As noted in Table 5, a higher yield surface intercept was deduced from fitting the long-term Rowe cell oedometer tests. Full details of the finite element analysis of the Gloucester test embankment are presented in Hinchberger and Rowe (1998) for the elliptical cap formulation and in Hinchberger (1996) for both formulations.

In Fig. 15, the field behaviour of the Gloucester test embankment is compared with calculated behaviour based on original Cam clay viscoplasticity and critical state parameters, M, of 0.9, 1.0, and 1.1. As noted above, the critical state parameter, M, of Gloucester clay is 0.9 (Law 1974). In Fig. 15, the calculated settlement below centerline of the Gloucester test embankment exceeds measured settlement at all depths when the correct critical state parameter $M = 0.9$ is used in the analysis. Agreement between calculated and measured settlement is improved by increasing the critical state parameter, M, to 1.1. The calculated behaviour could

Fig. 14. Summary of Gloucester stratigraphy and finite element input parameters.

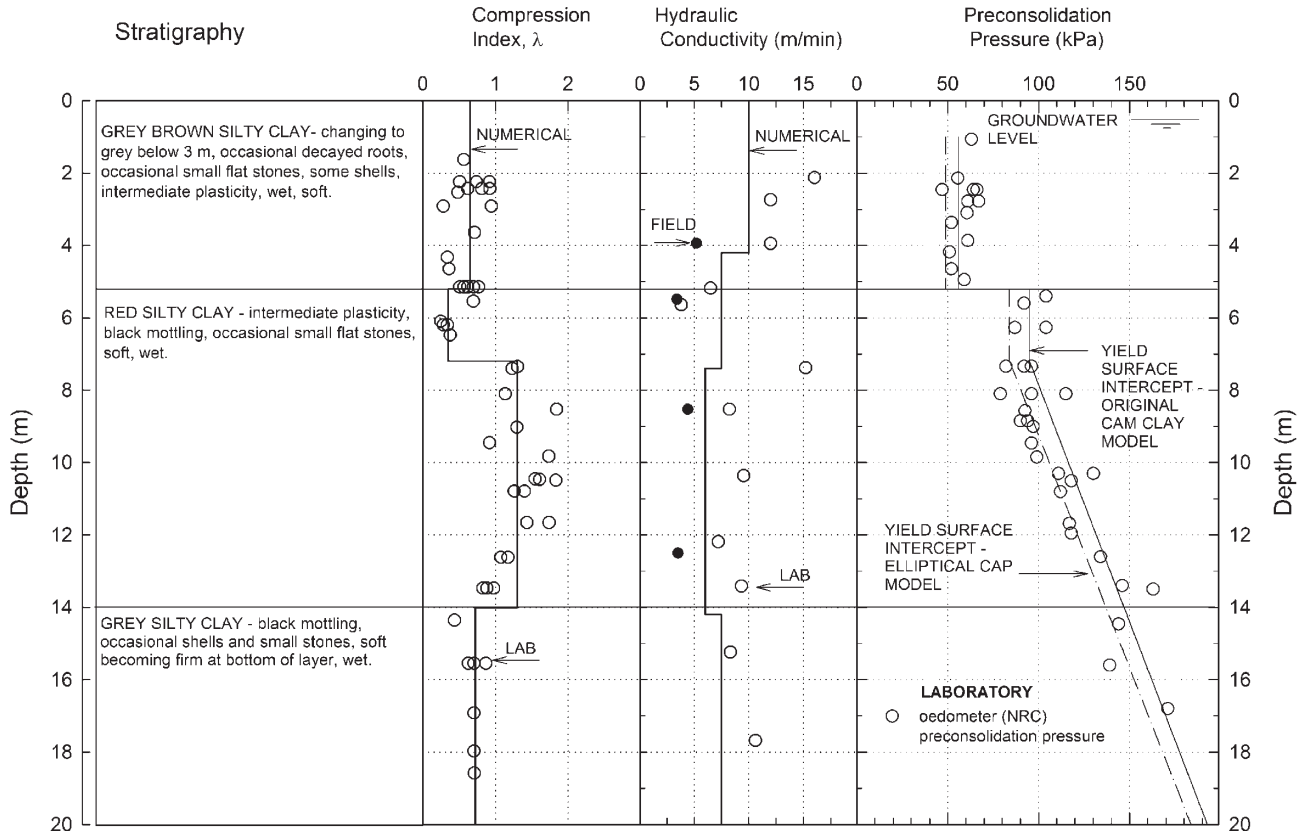

Table 6. Constitutive parameters for analysis of the Gloucester test embankment.

								Viscoplastic parameters			
Depth (m)	κ	λ	e_o	k_o ($\times 10^{-8}$ m/min)	C_k	k_h/k_v	v	γ^{vp} (s^{-1})	n	R	M
0–2	0.025	0.65	1.8	10.0	0.25	1.25	0.3	1.7×10^{-10}	28*/30†	1.65	0.9
2–5.2	0.025	0.65	1.8	7.2	0.25	1.25	0.3	1.7×10^{-10}	28/30	1.65	0.9
5.2–7.2	0.025	0.32	1.8	6.0	0.5	1.25	0.3	1.7×10^{-10}	28/30	1.65	0.9
7.2–13.4	0.025	1.35	2.4	6.0	0.25	1.25	0.3	1.7×10^{-10}	28/30	1.65	0.9
13.4–20.2	0.025	0.72	1.8	7.2	0.25	1.25	0.3	1.7×10^{-10}	28/30	1.65	0.9

Note: M = 0.9 for both models except as noted in Fig. 15. Cohesion intercept is zero, e.g., c'_{NC} = 0 kPa.
*Strain-rate parameter, n, for original Cam clay model.
†Strain-rate parameter, n, for elliptical cap model.

have also been improved by increasing the yield surface intercept; however, the resultant yield surface intercept profile would not be in agreement with the measured preconsolidation pressure profile (Fig. 14). The results in Fig. 15 have also been confirmed for instrumentation located below the embankment crest and toe (Hinchberger 1996).

In Fig. 16, the measured settlement below centerline of the Gloucester test embankment is compared with the calculated settlement for the elliptical cap formulation. In this case, there is reasonable agreement between the measured and calculated values. As discussed below, the improved behaviour of the elliptical cap model may be attributed to the yield surface shape.

Discussion

Overall, both constitutive models are shown to satisfactorily describe the behaviour of Sackville clay during CAU triaxial creep, CAU triaxial compression, and incremental oedometer consolidation tests. Compared with other soils in Fig. 1, the undrained shear strength of Sackville clay is considered to have a high degree of rate sensitivity. The ability of both constitutive formulations to describe the effect of strain rate on the undrained shear strength of Sackville clay is considered to be important in the study of embankments built to failure on rate-sensitive foundations. Only the elliptical cap formulation was found to be sufficiently flexible to simultaneously describe the rate-dependent behaviour of Sackville clay for the failure envelope parameters, c' and M, measured in triaxial compression (Gnanendran 1993).

The original Cam clay and elliptical cap models were then evaluated using the Gloucester case history (Bozozuk and Leonards 1972; Lo et al. 1976). The evaluation utilized laboratory data from long-term Rowe cell consolidation tests and

Fig. 15. Predicted and measured displacements at centerline for Stage 1 of the Gloucester test embankment: original Cam clay model.

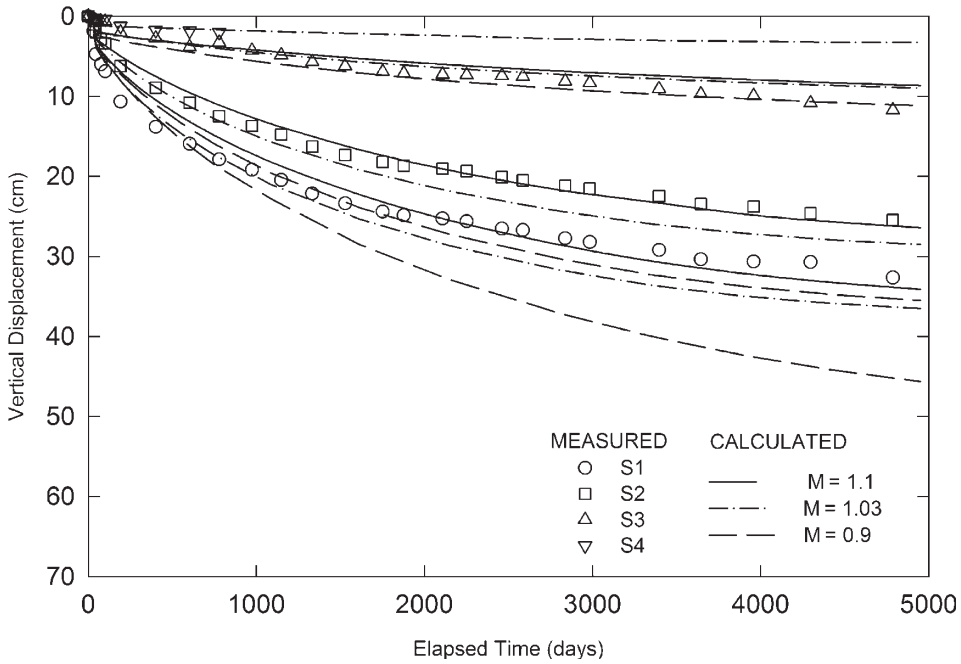

Fig. 16. Calculated and measured displacements at centerline for Stage 1 of the Gloucester test embankment: elliptical cap model.

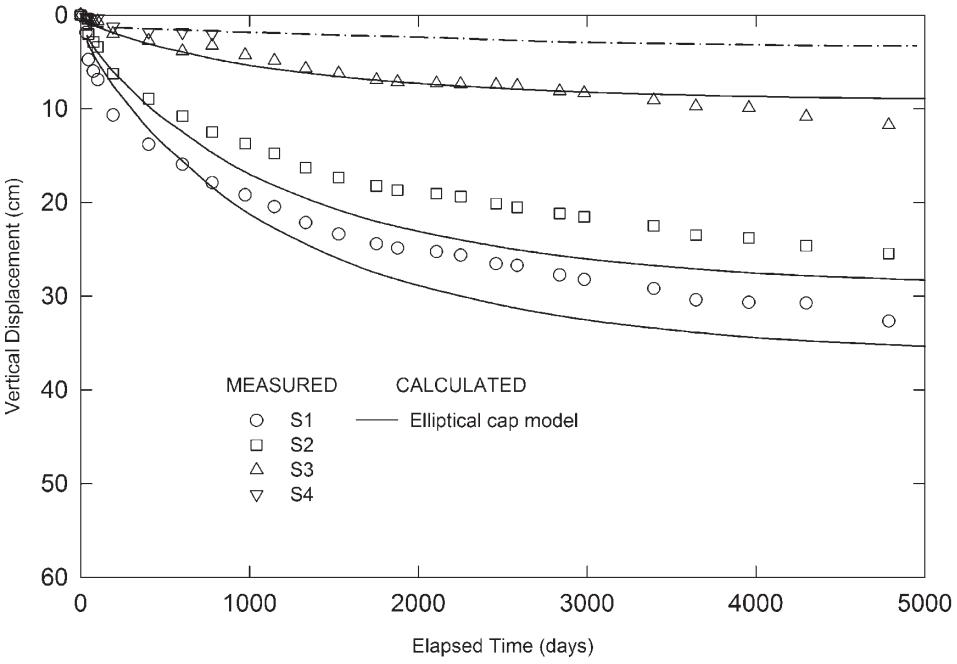

field data from the Gloucester case. Overall, both models were capable of describing the predominant rate-sensitive characteristics of Gloucester clay during long-term one-dimensional Rowe cell consolidation. In contrast, only the elliptical cap model was able to predict field behaviour using constitutive parameters that are consistent with laboratory tests. The original Cam clay model overestimated deformations during the 14 year record.

Figure 17 shows the stress path for a typical element of soil below centerline of the Gloucester test embankment. In addition, the initial and final position of the original Cam clay and elliptical cap yield surfaces are also shown in Fig. 17. For both formulations, the magnitude of volumetric plastic strain is proportional to the degree of yield surface expansion viz. eq. [4]. Thus, as shown in Fig. 17, for typical stress paths imposed by Stage I of the Gloucester test embankment, the original Cam clay yield surface predicts more volumetric plastic deformation than the elliptical cap yield surface. This is primarily due to the overall shape of the original Cam clay yield surface and it in part explains the inability of the original Cam clay model to adequately predict embankment settlements.

Fig. 17. Typical stress path and yield surface expansion of original Cam clay and elliptical cap yield surfaces 14 years after construction.

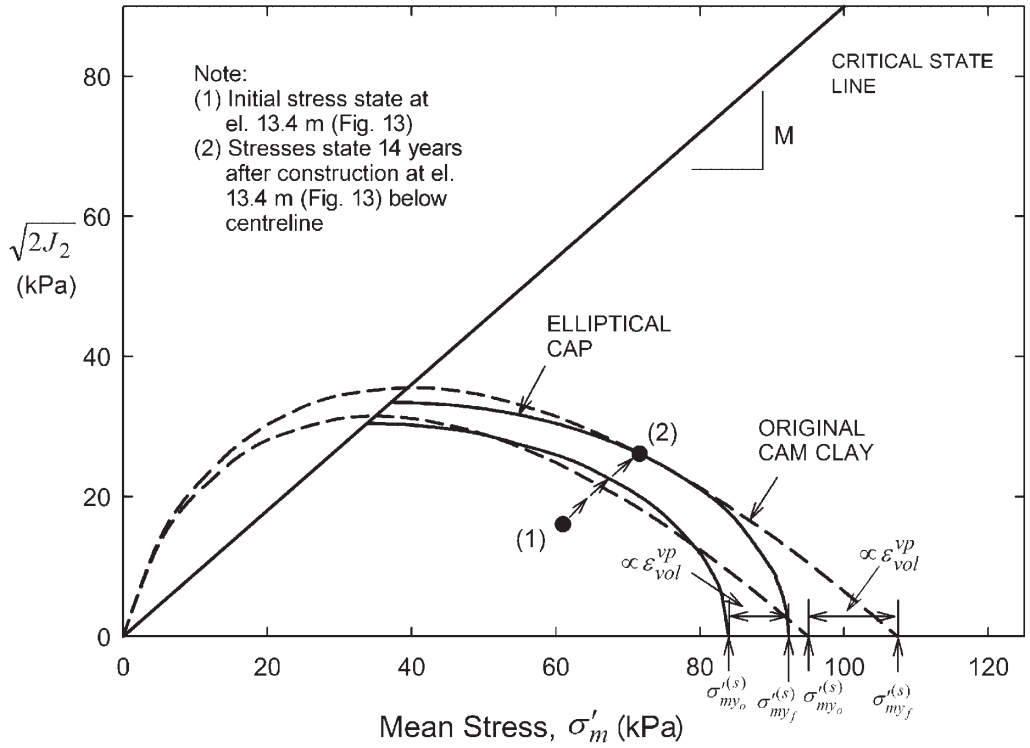

Although both formulations could be calibrated to describe the behaviour of Gloucester clay subject to a single stress path (e.g., oedometer consolidation), only the elliptical cap formulation was capable of simultaneously describing the response of Gloucester clay for the stress paths encountered during both laboratory and field loading. This is attributed primarily to the correct yield surface shape and the satisfactory time-dependent formulation. The original Cam clay model could be made to fit field behaviour of the Gloucester test embankment by adjusting the critical state parameter, M, and consequently the shape of the yield surface. However, this requires significant judgment to obtain good predictions and parameters that are not consistent with lab data.

In summary, the success of the elliptical cap formulation in describing the engineering response of Sackville and Gloucester clay may be attributed to the flexibility of both the elliptical yield surface and Drucker–Prager failure envelope, the time-dependent formulation adopted, and the limited anisotropy and structure exhibited by both clays over the range of strain rates mobilized during laboratory and field conditions. To adequately describe the two-dimensional constitutive response of Sackville and Gloucester clay, the following considerations were found to be important:

(*i*) A scalable elliptical yield surface, and

(*ii*) An overstress formulation capable of describing the apparent expansion of the yield surface in stress space due to changes in strain rate (dynamic stress path) for the dominant stress paths encountered during field and laboratory loading.

Both original Cam clay and elliptical cap formulations hypothesize the existence of a long-term or fundamental yield surface for clay that defines yield stress states corresponding to infinitesimal strain rates. Thus, there are practical limitations regarding the measurement of the long-term yield surface and consequent implications for the determination of constitutive parameters. In this paper, long-term creep tests have been used to estimate the position and shape of the long-term yield surface for Sackville clay. Similarly long-term oedometer tests were used for Gloucester clay. The majority of strain-rate effects appear to have been accounted for here; however, it is acknowledged that tertiary strain-rate processes have not been considered.

Conclusions

The predictive ability of two three-parameter elastic-viscoplastic formulations has been evaluated using two well-documented case histories involving embankments founded on soft rate-sensitive cohesive soils. Based on the detailed evaluation, the following conclusions are drawn:

(*i*) The elastic-viscoplastic constitutive models evaluated in this study appear to be capable of describing the influence of strain rate on the engineering behaviour of Sackville and Gloucester clay subject to drained and undrained loading.

(*ii*) For both models, viscoplastic constitutive parameters obtained from undrained tests are suitable for use in modeling clay behaviour during drained loading.

(*iii*) A constitutive formulation based on a scalable elliptical yield surface equation is required to describe both field and laboratory behaviour of Sackville and Gloucester clay subject to two-dimensional loading. Adopting a yield surface equation that cannot be scaled to account for variability of the c_u/σ'_p ratio of cohesive soils may result in significant error between calculated and measured behaviour.

(*iv*) The method of overstress measurement utilized for the elliptical cap model adequately describes the overstress

response of Sackville and Gloucester clay at yield and failure in laboratory and field loading conditions.

(*v*) The elliptical cap model evaluated in the present study appears to be suitable for use in the study of infrastructure built on soft rate-sensitive cohesive soils that do not exhibit significant strength anisotropy or structure.

Acknowledgements

The research reported in this paper was funded by a research grant from the Natural Sciences and Engineering Research Council of Canada.

References

Adachi, T., and Oka, F. 1982. Constitutive equations for normally consolidated clay based on elasto-viscoplasticity. Soils and Foundations, **22**(4): 57–70.

Adachi, T., and Okano, M. 1974. A constitutive equation for normally consolidated clay. Soils and Foundations, **14**: 55–73.

Biot, M.A. 1941. General theory of three-dimensional consolidation. Journal of Applied Physics, **12**: 155–164.

Bozozuk, M., and Leonards, G.A. 1972. The Gloucester test fill. Special Conference on Performance of Earth and Earth-Supported Structures, American Society of Civil Engineers, Purdue University, Lafayette, Ind. Vol. 1, Part 1, pp. 299–317.

Britto, A.M., and Gunn, M.J. 1987. Critical state soil mechanics via finite elements. Ellis Harwood, Chichester, UK.

Carter, J.P., and Balaam, N.P. 1995. AFENA– A general finite element algorithm: Users manual. School of Civil Engineering and Mining Engineering, University of Sydney, N.S.W. 2006, Australia.

Chen, W.F. 1982. Plasticity in reinforced concrete. McGraw-Hill, New York.

Davis, E.H. 1968. Theories of plasticity and failure of soil masses. *In* Soil mechanics– selected topics, Chapter 6. *Edited by* I.K. Lee. Butterworths, London.

Desai, C.S., and Zhang, D. 1987. Viscoplastic model for geologic materials with generalized flow rule. International Journal for Numerical and Analytical Methods in Geomechanics, **11**: 603–620.

Desai, C.S., Somasundaram, S., and Frantziskonis, G. 1986. A hierarchical approach for constitutive modeling of geologic materials. International Journal for Numerical and Analytical Methods in Geomechanics, **11**: 603–620.

Dittrich, P. 2002. Slope behaviour at Sarnia approach to the St. Clair Tunnel. Ph.D. thesis, Department of Civil and Environmental Engineering, The University of Western Ontario, London, Ont.

Folkes, D.J., and Crooks, J.H.A. 1985. Effective stress paths and yielding in soft clays below embankments. Canadian Geotechnical Journal, **22**: 357–374.

Fisher, D.G., Rowe, R.K., and Lo K.Y. 1982. Prediction of the second stage behaviour of Gloucester test fill. Geotechnical Research Report GEOT-4-82, The University of Western Ontario, Geotechnical Research Centre, London, Ont.

Fodil, A., Aloulou, W., and Hicher, P.Y. 1997. Viscoplastic behaviour of soft clay. Géotechnique, **47**(3): 581–591.

Gnanendran, C.T. 1993. Observed and calculated behaviour of a geotextile reinforced embankment on a soft compressible soil. Ph.D. thesis, Department of Civil Engineering, The University of Western Ontario, London, Ont.

Graham, J., Crooks, J.H.A., and Bell, A.L. 1983*a*. Time effects on the stress-strain behaviour of natural soft clays. Géotechnique, **33**(3): 327–340.

Graham, J., Noonan, M.L., and Lew, K.V. 1983*b*. Yield states and stress-strain relationships in a natural plastic clay. Canadian Geotechnical Journal, **20**: 502–516.

Hinchberger, S.D. 1996. The behaviour of reinforced and unreinforced embankments on soft rate-sensitive foundation soils. Ph.D. thesis, Department of Civil Engineering, The University of Western Ontario, London, Ont.

Hinchberger, S.D., and Rowe, R.K. 1998. Modelling the rate-sensitive characteristics of the Gloucester foundation soil. Canadian Geotechnical Journal, **35**: 769–789.

Janbu, N. 1963. Soil compressibility as determined by oedometer and triaxial tests. *In* Proceedings of the 2nd European Conference on Soil Mechanics and Foundation Engineering, Problems of Settlements and Compressibility of Soils. Wiesbaden, Germany. *Edited by* Deutsche Gesellschaft fuer Erd-und Grundbau. Vol. 1, pp. 19–25.

Katona, M.G., and Mulert, M.A. 1984. A viscoplastic cap model for soils and rock. Chapter 17. *In* Mechanics of engineering material. *Edited by* C.S. Desai and R.H. Gallagher. J. Wiley, London.

Kavazanjian, E., Jr., Borja, R.I., and Jong, H.L. 1985. Time-dependent deformation of clays. Journal of Geotechnical Engineering, ASCE, **106**(GT6): 611–630.

Kim, Y.T., and Leroueil, S. 2001. Modeling the viscoplastic behaviour of clays during consolidation: application to Berthierville clay in both laboratory and field conditions. Canadian Geotechnical Journal, **38**: 484–497.

Kutter, B.L., and Sathialingam, N. 1992. Elastic-viscoplastic modeling of the rate-dependent behaviour of clays. Géotechnique, **42**(3): 427–441.

Lagioia, R., Puzrin, A.M., and Potts, D.M. 1996. A new versatile expression for yield and plastic potential surface. Computers and Geotechnics, **19**(3): 171–191.

Law, K.T. 1974. Analysis of embankments on sensitive clays. Ph.D. thesis, Department of Civil Engineering, The University of Western Ontario, London, Ont.

Leroueil, S. 1997. Critical state soil mechanics and the behaviour of real soils. *In* Proceedings of the International Symposium on Recent Developments in Soil and Pavement Mechanics, Rio de Janeiro, Brazil, 25–27 June 1997. *Edited by* M.S.S. Almeida, A.A. Balkema, Rotterdam, The Netherlands. pp. 41–80.

Leroueil, S., Sampson, L., and Bozozuk, M. 1983. Laboratory and field determination of preconsolidation pressures at Gloucester. Canadian Geotechnical Journal, **20**: 477–490.

Lo, K.Y., Bozozuk, M., and Law, K.T. 1976. Settlement analysis of the Gloucester test fill. Canadian Geotechnical Journal, **13**: 339–354.

Massachusetts Institute of Technology (M.I.T.). 1975. Proceedings of the Foundation Deformation Prediction Symposium. U.S. Department of Transportation, Report FHWA-RD-75-515. Vol. 1 and 2.

Mitchell, R.J. 1970. On the yielding and mechanical strength of Leda clays. Canadian Geotechnical Journal, **7**: 297–312.

Norton, F.H. 1929. Creep in steel at high temperatures. McGraw-Hill Book Co., New York.

Oka, F., Adachi, T., and Okano, Y. 1986. Two-dimensional consolidation analysis using an elasto-viscoplastic constitutive equation. International Journal for Numerical and Analytical Methods in Geomechanics, **10**: 1–16.

Pastor, M., Zienkeiwicz, O.C., and Chan, A.H.C. 1990. Generalized plasticity and the modeling of soil behaviour. International Journal for Numerical and Analytical Methods in Geomechanics, **14**: 151–190.

Perzyna, P. 1963. The constitutive equations for work-hardening

and rate sensitive plastic materials. Proceedings of Vibrational Problems, Warsaw, **4**(3): 281–290.

Rocchi, G., Fontana, M., and Da Prat, M. 2003. Modelling the natural soft clay destruction processes using viscoplasticity theory. Géotechnique, **53**(8): 729–745.

Roscoe, K.H., and Burland, J.B. 1968. On the generalized stress-strain behaviour of "wet" clay. *In* Engineering plasticity. Cambridge University Press, Cambridge, Mass.

Roscoe, K.H., and Schofield, A.N. 1963. Mechanical behaviour of an idealized "wet clay." *In* Proceedings of the 2nd European Conference on Soil Mechanics and Foundation Engineering. Problems of Settlements and Compressibility of Soils, Wiesbaden, Germany. *Edited by* Deutsche Gesellschaft fuer Erd-und Grundbau. pp. 47–54.

Rowe, R.K., and Hinchberger, S.D. 1998. The significance of rate effects in modelling the Sackville test embankment. Canadian Geotechnical Journal, **33**: 500–516.

Rowe, R.K., Gnanendran, C.T., Landva, A.O., and Valsangkar, A.J. 1995. Construction and performance of a full-scale geotextile reinforced test embankment, Sackville, New Brunswick. Canadian Geotechnical Journal, **32**: 512–534.

Rowe, R.K., Gnanendran, C.T., Landva, A.O., and Valsangkar, A.J. 1996. Calculated and observed behaviour of a reinforced embankment over soft compressible soil. Canadian Geotechnical Journal, **33**: 324–338.

Sheahan, T.C., Ladd, C.C., and Germaine, J.T. 1996. Rate-dependent undrained shear behaviour of saturated clay. Journal of Geotechnical and Geoenvironmental Engineering, ASCE, **122**(2): 99–108.

Tavenas, F., and Leroueil, S. 1977. Effects of stresses and time on yielding of clays. *In* Proceedings of the 9th International Conference on Soil Mechanics and Foundation Engineering, Tokyo, 11–15 July 1997. Japanese Society of Soil Mechanics and Foundation Engineering, Tokyo, Japan. Vol. 1, pp. 319–326.

Tavenas, F., Jean, P., LeBlond, P., and Leroueil, S. 1983. The permeability of natural soft clays. Part II: Permeability characteristics. Canadian Geotechnical Journal, **20**: 645–660.

Vaid, Y.P., Robertson, P.K., and Campanella, R.G. 1979. Strain rate behaviour of Saint-Jean Vianney clay. Canadian Geotechnical Journal, **16**: 34–42.

Wedage, A.M.P., Morgenstern, N.R., and Chan, D.H. 1998. A strain rate dependent constitutive model for clays at residual strength. Canadian Geotechnical Journal, **35**: 364–373.

Yin, J.-H., Zhu, J.-G., and Graham, J. 2002. A new elastic viscoplastic model for time-dependent behaviour of normally and overconsolidated clays: theory and verification. Canadian Geotechnical Journal, **39**: 157–173.

Zhu, G., Yin, J.-H., and Graham, J. 2001. Consolidation modelling of soils under the test embankment at Chek Lap Kok International Airport in Hong Kong using a simplified finite element method. Canadian Geotechnical Journal, **38**: 349–363.

List of symbols

C_α coefficient of secondary compression
C_c virgin compression index
C_k slope of e – log (k) plot
c_u undrained shear strength
c' effective cohesion intercept in τ–σ' stress space
c'_{NC} Drucker–Prager cohesion intercept in $\sqrt{2J_2} - \sigma'_m$ stress space; normally consolidated range
c'_{OC} Drucker–Prager cohesion intercept in $\sqrt{2J_2} - \sigma'_m$ stress space; overconsolidated range
e void ratio
e_o reference void ratio for e – log (k) relationship
$\partial g/\partial \sigma'_{ij}$ plastic potential
G shear modulus
J_2 second invariant of deviatoric stress tensor (= $1/6[(\sigma'_{11} - \sigma'_{22})^2 + (\sigma'_{11} - \sigma'_{33})^2 + (\sigma'_{22} - \sigma'_{33})^2] + \sigma^2_{12} + \sigma^2_{13} + \sigma^2_{23}$)
k hydraulic conductivity
k_h, k_v horizontal and vertical hydraulic conductivity, respectively
K bulk modulus of elasticity
k_o reference hydraulic conductivity for e – log (k) relationship
K'_o coefficient of lateral earth pressure at rest
l σ'_m coordinate of the centre of the elliptical yield surface function
M slope of Drucker–Prager failure envelope in $\sqrt{2J_2} - \sigma'_m$ stress space; normally consolidated stress range
M_{OC} slope of Drucker–Prager failure envelope in $\sqrt{2J_2} - \sigma'_m$ stress space; overconsolidated stress range
n viscoplastic strain rate exponent
R elliptical yield surface aspect ratio in $\sqrt{2J_2} - \sigma'_m$ stress space
R_k ratio of horizontal to vertical permeability (= k_H/k_v)
s_{ij} deviatoric stress tensor
u_e excess pore pressure
v Poisson's ratio
w_L liquid limit (%)
w_N natural water content (%)
w_P liquid limit (%)
γ bulk unit weight
γ_{fill} bulk unit weight of embankment fill
γ^{vp} fluidity constant for viscoplastic analysis
δ_{ij} Kronecker's delta
$\partial \varepsilon^{vp}_{vol}$ incremental volumetric viscoplastic strain
$\dot{\varepsilon}_{axial}$ axial strain rate
$\dot{\varepsilon}^{e}_{ij}$ elastic strain rate tensor
$\dot{\varepsilon}^{vp}_{ij}$ viscoplastic strain rate tensor
$\dot{\varepsilon}_{ij}$ total strain rate tensor
$\dot{\varepsilon}^{vp}_{vol}$ volumetric viscoplastic strain rate
κ recompression index
λ compression index
σ' effective stress
$\sigma'^{(d)}_{my}$ dynamic yield surface intercept
$\sigma'^{(d)}_{OS}$ overstress
$\sigma'^{(s)}_{my}$ static yield surface intercept
σ'_{ij} effective stress tensor
σ'_m mean effective stress (= $(\sigma'_1 + \sigma'_2 + \sigma'_3)/3$)
σ'_p preconsolidation pressure
$\phi(F)$ viscoplastic flow function
ϕ' effective friction angle (Mohr–Coulomb failure envelope)
ψ angle of dilatancy